Dynamic bending of an ice wedge resting on a winkler-type elastic foundation

Jeong-Hwan Kim, Wenjun Lu, Raed Lubbad, Sveinung Løset, Beom-Seon Jang

PII: S0165-232X(22)00098-2

DOI: https://doi.org/10.1016/j.coldregions.2022.103579

Reference: COLTEC 103579

To appear in: *Cold Regions Science and Technology*

Received date: 2 December 2020

Revised date: 10 January 2022

Accepted date: 25 April 2022

Please cite this article as: J.-H. Kim, W. Lu, R. Lubbad, et al., Dynamic bending of an ice wedge resting on a winkler-type elastic foundation, *Cold Regions Science and Technology* (2021), https://doi.org/10.1016/j.coldregions.2022.103579

Dynamic Bending of an Ice Wedge Resting on a Winkler-type Elastic Foundation

Jeong-Hwan Kim[1,2]*, Wenjun Lu[3]*, Raed Lubbad[4], Sveinung Løset[5], Beom-Seon Jang[6]

[1]Department of Naval Architecture and Offshore Engineering, Dong-A University, Busan, South Korea (jhkim81@dau.ac.kr, Assistant professor)

[2]Research Institute of Marine Systems Engineering, Seoul National University, Seoul, South Korea

[3]Department of Civil and Environmental Engineering, Norwegian University of Science and Technology, Trondheim, Norway (wenjun.lu@ntnu.no, Senior researcher)

[4]Department of Civil and Environmental Engineering, Norwegian University of Science and Technology, Trondheim, Norway (raed.lubbad@ntnu.no, Associate professor)

[5]Department of Civil and Environmental Engineering, Norwegian University of Science and Technology, Trondheim, Norway (sveinung.loset@ntnu.no, Professor)

[6]Department of Naval Architecture and Ocean Engineering, Seoul National University, Seoul, South Korea (seanjang@snu.ac.kr, Associate professor)

Abstract

For most ice – sloping structure interactions, the incoming ice floes' failures are determined by the formation of circumferential cracks. This physical process can be simplified as analyzing the bending failure of an ice wedges resting on a fluid foundation. In history, closed-form analytical/empirical solutions have been developed for the static bending problem; and numerical solutions have been attempted for the dynamic scenarios. This paper revisits this classic problem and conducts extensive Finite Element Method (FEM) – based simulations on the dynamic bending of an ice wedge resting on a Winkler-type elastic foundation. The simulations are based on inputs (i.e., ice wedge geometry, loading radius and loading rate) within ranges that are typical for engineering applications. Based on the simulation, a database of 'ice breaking load' and 'ice breaking length' is constructed. Then we applied the Artificial Neural Network (ANN) method to establish the general relationship between the varying inputs (i.e., ice wedge angle, loading radius and rate) with the target outputs (i.e., breaking load and length). Such relationship is expressed in simple closed-form (i.e., Eq. (13)) allowing for easy, efficient and wide engineering applications. In the process of developing the ANN model, based on extensive FEM-simulations, we managed to extend Nevel's (1972) analytical solution. We also quantitatively demonstrated many well-known dynamic effects in this classic problem, e.g., a faster loading rate leads to a larger ice breaking load and a shorter ice breaking length. In addition, we also uncovered the failure pattern transition of an ice wedge, i.e., when an ice wedge's angle is below 100°, the circumferential crack will develop first; however, when the ice wedge gets wider than around 100°, depending on the loading radius and interaction velocity, the radial crack is more prone to develop first.

Keywords: out-of-plane failure; dynamic bending; ice – structure interactions; ANN model; icebreaker

1. Introduction

Bending failures of sea ice plays a key role in ice-structure interactions. Most Arctic offshore structures (e.g., icebreakers and offshore structures) are designed with a sloping surface at the ice line (Ashton, 1986). Because ice is easier to fail in tension than in compression, the sloping surface induces the bending failure of incoming ice floe. This leads to reduced total ice load. The bending failure of sea ice can be categorized as a type of out-of-plane failure modes (Lu et al., 2016), in which, the ice cover can be theorized as an elastic plate resting on a Winkler-type elastic foundation (Lu et al., 2015, Kerr and Palmer, 1972, Lilja et al., 2019, Ashton, 1986, Kerr, 1976, Langhorne et al., 1999, Michel, 1978, Sodhi et al., 1982, Sodhi, 1983, Sodhi, 1997, Squire et al., 1996). The out-of-plane failure of a floating ice sheet has been observed to take two stages. The first stage is the so-called radial cracking of the ice floe (i.e., radial cracks emanating from the vertically loaded area and intersecting an ice sheet into several ice wedges); the second stage is the formation of circumferential cracks some distance away from the vertically loaded area. It is generally accepted that the closest circumferential crack's formation corresponds to the maximum ice load. Therefore, the original problem of the out-of-plane failure of an ice sheet are reduced to the analysis of several ice wedge bending failures, e.g., (Nevel, 1958, Nevel, 1961, Nevel, 1972, Bažant, 1992, Bažant and Li, 1993, Bažant and Li, 1994, Li and Bažant, 1994). However, most existing and widely used ice wedge bending solutions are based on static solutions.

The dynamic bending of an ice wedge was numerically studied by several authors (Sawamura et al., 2008, Sawamura et al., 2010, Lu et al., 2012b, Lu et al., 2012a). It was evident that the dynamic effects significantly influence the ultimate ice breaking load f_b and ice breaking length l_b. Until now, only Sawamura et al. (Sawamura et al., 2009, Sawamura, 2014) manage to tabulate the numerical results to simulate ship-ice interactions. Comparing with the analytical/empirical solutions, numerical simulations are rather time-consuming; and the tabulated results are not general enough for all/most engineering applications. Given the importance of the dynamic effect and the desire of having more general results for wider applications, this paper aims to produce a set of general solutions in 'closed form' to solve the dynamic ice wedge bending problem with Finite Element Modelling (FEM) and Artificial Neural Network (ANN).

ANN is a tool that enables multivariate nonlinear regression to efficiently model complex systems without any prior assumptions (Sharifi and Mohebbi, 2012). Kim et al. (2020) predicted the ice resistance of ice-going vessels in level ice using a data-driven model based in the ANN model. They trained the model by various parameters, i.e., varying ship geometries and environmental conditions, and the model was validated against

field measurements. Li et al. (2020) built a model to estimate ship-ice interaction of shoulder and midship areas using FE based ANN technique. The model shows fast calculation speed as analytical formulae and high accuracy as numerical modelling.

1.1 Widely used early static solutions

For ship-ice/ice-structure interactions, previous researchers, e.g.,(Kotras et al., 1983, Naegle, 1980, Lindqvist, 1989, Kämäräinen, 2007, Valanto, 2001, Lu et al., 2015), have identified at least three major interaction phases and several ice load components. These are: 1) the ice breaking phase, in which, ice wedge bending failure takes place; 2) the ice rotating phase, in which the broken ice piece was rotating until it becomes parallel to the ship hull; and 3) the ice rubble sliding phase, in which, ice rubbles slide along the ship hull. In the context of ice structure interactions, the state-of-art technique to characterize the ice wedge bending failure is based on empirical and/or analytical solutions. For example, Kashtelian's work in Eq. (1) are extensively referenced in the work of (Su et al., 2010a, Su et al., 2010b, Su et al., 2010c, Zhou et al., 2011, Tan et al., 2013) to simulate ship and level ice interactions; and Nevel's solution (Nevel, 1958, Nevel, 1972) are utilized in the Nonsmoothed Discrete Element Method (NDEM) based simulators (Metrikin and Løset, 2013, Lubbad and Løset, 2011, Septseault et al., 2014, Dudal et al., 2015) to calculate level ice bending failures. An adaptation (from (Lu et al., 2016)) of Nevel's solution is presented in Eq. (2).

$$f_b = C_f(\frac{\theta}{\pi})^2 \sigma_f h^2 \tag{1}$$

in which,

f_b is the maximum vertical force that leads to the bending failure of an ice wedge, in [kN];

θ is the angle of the ice wedge, in [rad];

σ_f is the flexural strength of the ice material, in [kPa];

h is the ice thickness, in [m];

C_f is an empirical coefficient, in [-].

$$f_b = \frac{\theta}{\pi}\frac{2}{3}\sigma_f h^2[1.05 + 2.0(\frac{a}{l_c}) + 0.5(\frac{a}{l_c})^3] \tag{2}$$

in which,

a is loading radius (see Fig. 1), in [m];

l_c is defined in Eq. (4) and is the characteristic length of floating ice plate, in [m];

These formulas are primarily intended for quasi-static scenarios; and the maximum force when an ice wedge fails depends only on the geometrical factors (a, θ and h) and material properties (σ_f and l_c). The interaction velocity and inertia from both the solid ice and fluid foundation are not included in these formulas. However, due to their simplicity, they are widely used in the simulation of ice – structure interaction simulations to characterize the ice bending failure.

1.2 Dynamic effects

Following the formulation stated in Dempsey and Zhao (1993), the current dynamic ice wedge bending problem can be formulated as in Eq. (3).

$$\rho_i h \frac{\partial^2 w'}{\partial t^2} + D\nabla^4 w' + p_0' = \frac{f_b}{\theta a}\delta(r' - a) \tag{3}$$

in which,

ρ_i is the ice density [kg/m^3];

w' is the local deflection (in [m]) and is a function of $w'(r', \theta)$;

r' is the distance (in [m]) to the tip of ice wedge in the polar coordinate system referring to Fig. 1;

D is the flexural rigidity of the plate and $D = \frac{Eh^3}{12(1-\zeta^2)}$; with E being the Young's modulus, ζ is Poisson ratio;

p_0' is the pressure from the fluid foundation.

The dynamic effects stem from two sources. One is the inertia of the solid ice (i.e., $\rho_i h \frac{\partial^2 w'}{\partial t^2}$) and the second is the hydrodynamic effect from the fluid foundation p_0'. The hydrodynamic influence from the fluid foundation is rather complicated. The potential theory has been applied to calculate this effect in conjunction with plate or beam theories (Dempsey and Zhao, 1993, Valanto, 2001, Keijdener et al., 2018). For the ice wedge bending problem, the fluid foundation together with the ice wedge have been simulated with the Finite Element Method (FEM) (Sawamura et al., 2008, Lu et al., 2012a).

In the present study, we limit ourselves to the study of considering the inertia effect from the ice wedge only; and simplify the reaction from the fluid foundation with the Winkle-type foundation. This means the term p_0' in

Eq. (3) is replaced with $p_0' = \rho_w g w'$, in which, ρ_w is the water density [kg/m^3] and $g = 9.81$m/s^2. With this simplification, we can define the characteristic length l_c as in Eq. (4).

$$l_c = \left(\frac{D}{\rho_w g}\right)^{\frac{1}{4}} \tag{4}$$

The Partial Differential Equation (PDE) in Eq. (3) will be solved by FEM in this paper. It is expected that a higher loading rate will lead to a higher ultimate ice breaking load f_b and a shorter ice breaking length l_b. It should be noted that by adopting the Winkle-type foundation, we are not capturing the entire dynamic effects in the ice wedge bending problem. This is a first step towards the more sophisticated treatment of the hydrodynamic effects of the fluid foundation in forthcoming studies.

This paper is arranged as following: in Section 2, the FEM-based numerical model to simulate the current ice bending problem is presented. It concerns mainly the method to solve Eq. (3) in extracting the ice breaking force f_b and ice breaking length l_b. We also present in Section 2 an ANN model to generalize the simulated results. In Section 3, an extensive simulation matrix is established to generate sufficient data, based on which, the ANN model will be utilized to produce more general solutions to the current problem. For the results of this paper, we first present the FEM-based numerical results in Section 4, which include validations against static solutions (Section 4.1) and the dynamic results (Section 4.2). Then in section 5, we present the derived ANN model. In section 6, we present the validation of the derived ANN model against existing numerical results (Section 6.2) and experimental results (Section 6.3). In the end, the results are discussed in Section 7 and conclusions are made in Section 8 of the paper.

2. Methodology

2.1 Finite element models for ice breaking simulation

The purpose is to establish a 'data base' of ice breaking force and length by simulating the bending failure of ice wedges with varying wedge angles, loading radius and rates. The simulation method is based on the Finite Element Method (FEM). Before carrying out massive simulations, we first verified the constructed FEM model

against known analytical solutions. The verification process involves solving the constructed FEM model with the static solver (i.e., ABAQUS/Standard 2017). The obtained static solutions are compared with available analytical solutions, which is static. After the successful static benchmarking simulations, the same model is simulated with the dynamic solver (i.e., ABAQUS/Explicit 2017) with varying loading rates and wedge geometries to explore the dynamic effects on the maximum bending failure force and ice breaking length.

2.1.1 Numerical model description

Load and boundary conditions of the numerical model used in this study are described in Fig. 1. Regarding the length of the wedge model, Sodhi (1996) showed that radial cracks do not exceed twice the maximum characteristic length l_c. The analyses by Lu et al. (2015) also showed that when an edge loaded plate's size is larger than about $4l_c$, the results start to converge to the semi-infinite plate solutions. In this study, the length of ice wedge is set to be $4l_c$. This is the same as in previous studies, e.g., Lu et al. (2012) and Spencer (1993) chose $4l_c$ as the ice wedge length to minimize the influence of boundary effects while at the same time limiting the simulation domain. As mentioned before, the fluid foundation is idealized as a Winkle-type foundation. For the static analysis using ABAQUS/Standard, we applied the built-in Winker-type boundary condition; for the dynamic analysis, as ABAQUS/Explicit does not have such a built-in function, a specific user-subroutine was programmed (with Fortran) to realize the Winker-type foundation. We have compared both approaches in a comparable quasi-static scenario and they show almost identical results, signifying the correctness of our implemented user-subroutine. As for the load, a constant pressure P_c is applied to the area with a loading radius 'a' shown in Fig. 1. The load is made to increase proportionally with time. When the first circumferential crack appears, the peak force is set as the breaking force f_b; and the distance between the wedge tip to the crack is output as the ice breaking length l_b. General inputs for the simulation model are presented in Table 1. Note that the presented results are nondimensionalized such that they are applicable to more general scenarios. The exact numerical numbers in Table 1 are only adopted for the sake of numerical simulations.

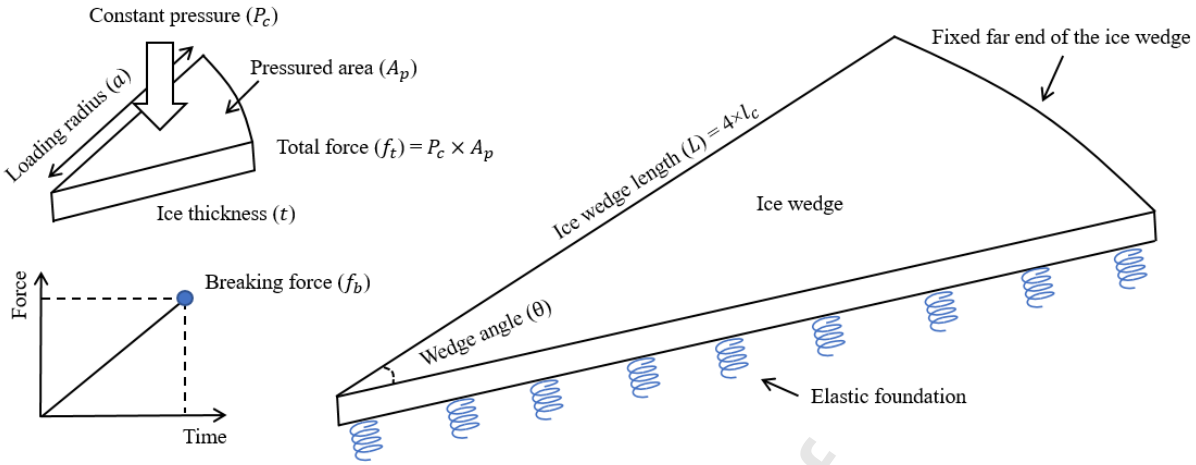

Fig. 1 Numerical model description.

Table 1 General inputs for the simulation.

Young's Modulus E	3.5 GPa
Possion ratio υ	0.3
Density of ice ρ_i	900 kg/m^3
Density of water ρ_w	1025 kg/m^3
Ice wedge thickness h	1 m
Ice wedge length L	is chosen as 54 m since $4l_c$=4×$\sqrt[4]{\frac{D}{\rho_w g}}$=53.45 m

As introduced before, the ultimate failure of an ice wedge is controlled by fracture initiation. This means that once the simulated stress reaches the critical material strength (i.e., tensile strength), the ice wedge can be assumed to have failed. This corresponds to the first circumferential crack on the ice wedge. It means that we just need to simulate our problem up to the point of 'fracture initiation' to extract the peak force f_b and ice breaking length l_b. However, in order to have a more visually appealing simulation results, we introduced a damage model to simulate the post-failure behavior of the ice wedge. It should be noted here that the choice of the damage model can be arbitrary as it does not influence f_b and l_b. In this paper, we chose the hyperbolic Drucker-Prager model, which is a modification of the linear Drucker-Prager model as shown in Fig. 2. Parameters for the Drucker-Prager plasticity model are as follows:

d' is the internal cohesion term, and 600 kPa was used in this study;

β is the friction angle, and 45° was used in this study;

p is the hydrostatic part of the stress tensor σ;

q is the equivalent stress with the deviatoric part of the stress tensor σ;

p_t is assumed to be half of the uniaxial tensile strength (250 kPa) because no triaxial tensile strength data of sea ice are available

The fracture evolution follows the cohesive zone model and fracture are explicitly 'expressed' with the element erosion technique for the simulation.

Simply put, this redundant post-failure simulation follows the following step:

- When the material reaches the yield criterion (characterized by the hyperbolic Drucker-Prager model), it follows a perfect plasticity flow rule until the equivalent plastic strain reaches 30 % of the elastic strain.
- Regarding the damage evolution law, it follows the cohesive zone model with a linear softening curve.

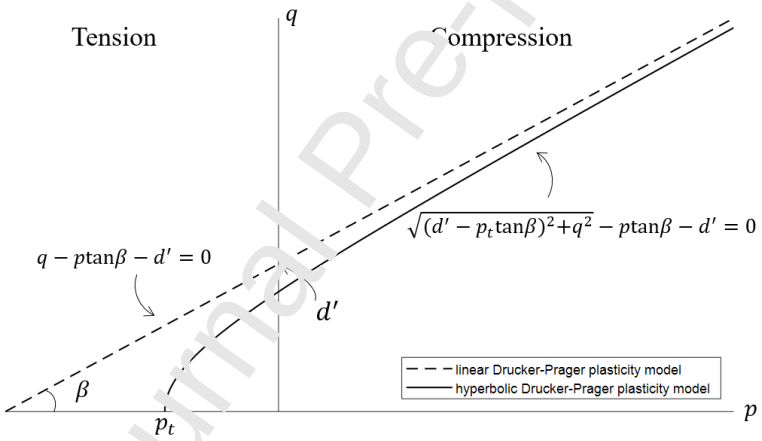

Fig. 2 Drucker-Prager plasticity models

It should be re-iterated that the above fracture evolution simulation is only for visual purpose. They do not necessarily reflect the truth of ice material in its failing process; and they do not influence our interested results, i.e., f_b and l_b, which are governed by pre-failure processes.

2.1.2 Mesh sensitivity study

The eight-node linear brick element with reduced integration (C3D8R) was used for the simulation of the three-

dimensional ice wedges. When the model is carrying bending loads, enough layers of the brick elements should be made through the thickness since the element has only one integration point with limited capacity to characterize the bending stress/deformation. In addition, it is known that the element sizes in the radial and circumferential directions also influence the results according to the geometrical features of the wedge. Lu et al (2012) presented that for the current problem, there should be more than four layers of elements in the thickness direction; and it is more affected by the element size in the circumferential direction than in radial direction. This is because the ice wedge is usually broken by radial stress (σ_{rr}) forming a circumferential crack (See the local coordinate system in Fig. 3).

A mesh sensitivity study has been carried out for the wedge model whose angle is 45° and thickness is 1 m. The mesh size in the thickness- and radial- directions are set to be equal. In the circumferential direction, the ice wedge are meshed with a mesh interval of one to two degree with considerations of individual element's aspect ratio. The number of elements layers in the thickness direction is varied between 4 to 6. The center line of the wedge is taken as a reference line (see Fig. 4). The radial stress σ_{rr} along the reference line is presented in Fig. 4. The results are compared with Nevel's analytical solution. It transpires that the five-layer mesh model approximates Nevel's solution best. Given this result, we choose the five-layer mesh model in all forthcoming simulations. Fig. 5 shows an example of FEM mesh used in the simulation.

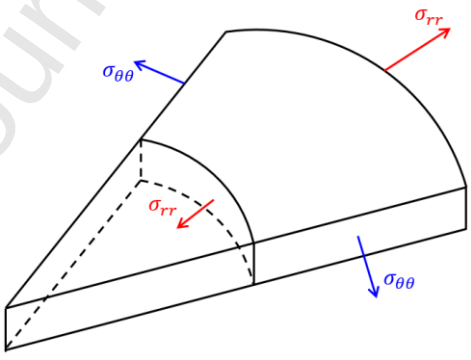

Fig. 3 Local cylindrical coordinate system of ice wedge model

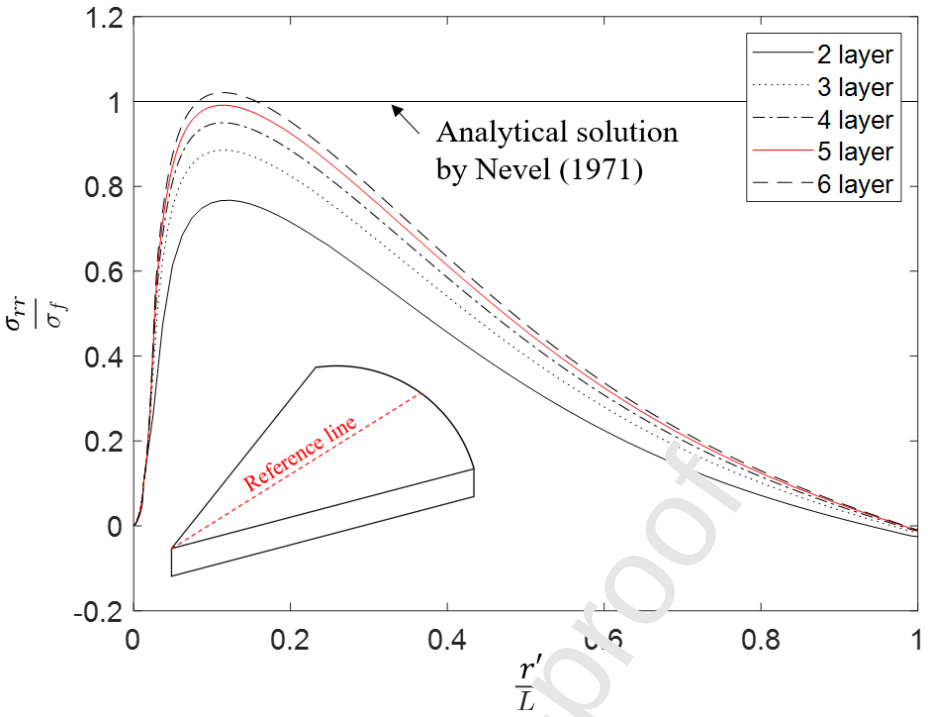

Fig. 4 Result of mesh sensitivity study

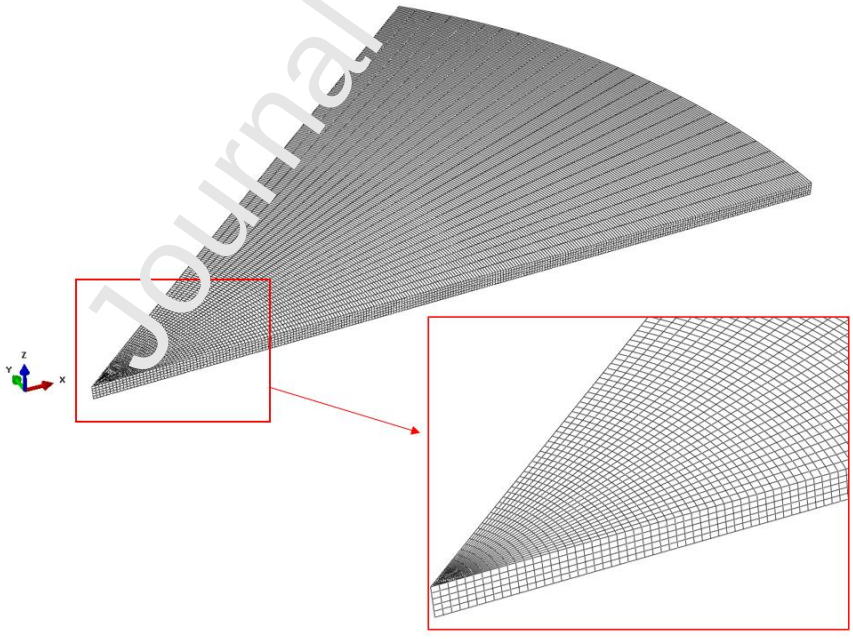

Fig. 5 Example of FEM mesh (wedge angle: 45°)

2.2 Prediction model using the Artificial Neural Networks

Ideally, one would prefer to obtain analytical solutions to Eq. (3). However, this is rather challenging if it is possible at all given the current application. One way of generalizing the results is to tabulate the discrete numerical results in a table or graph from where other scenarios can be extracted/interpolated/extrapolated. This approach has been developed and applied by Sawamura et al. (2009, 2014).

One of the novelties from this paper is that we adopt a different approach (the ANN model) to generalize the numerical results in this study. Generally, no matter how complex a physical process is, as long as its field variables are smooth enough, an 'analytical' model can be established based on the numerical simulation analyses. The input variables and simulation outputs can be 'linked' through a much-simplified equation. This simplified equation will be valid at least in the region where the data points are supplied. Traditionally, this can be achieved by the multi regression technique and the dimension reduction technique. However, these methods suffer when there are many variables and their relationships are highly nonlinear. There is an artificial neural network technique that is suitable for implementing a multivariate and nonlinear system. Fig. 6 shows the basic ANN structure. Artificial neural network, as its name suggests, is a collection of numerous artificial neurons. Each neuron is connected to the neighboring neurons by weight and transmits signals. The model is trained by the process of mapping the input to the output through each layer. As this process is repeated several times, the weights of each neuron are determined. As the number of iterations of training increases, the more accurate weights can be obtained. Therefore, a sufficient number of data is usually required for the construction of an ANN model. The data are normally divided into three parts, i.e. training, validation and testing datasets. First, the model calculates the weight between each neuron using the training dataset. This can be understood as a process of deriving the coefficient of an equation in general regression. Then, the performance of the trained model is calculated based on the validation dataset, and each parameter is modified to preventing overfitting. After these two steps, the development of the ANN model is completed. The performance of the developed model is evaluated by the last remaining test dataset. The detailed method used in this study is presented with actual data in Section 5.

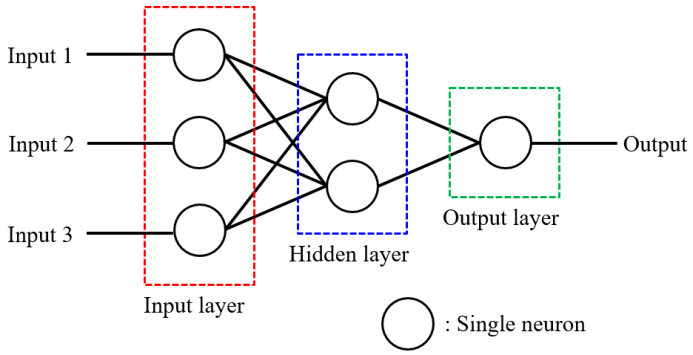

Fig. 6 Basic structure of the Artificial neural network (ANN) model

3. Numerical test matrix

The numerical tests that have been carried out are listed in Table 2. The parameters considered in the numerical tests are the loading radius, wedge angle and interaction velocity. In this paper, we normalize all length scales with the characteristic length to yield more general numerical results. The loading radius (a/l_c) varies from 0.05 to 1.0 with 0.05 interval. In case of the wedge angle, six cases in the range of from 30° to 100° are taken into account. The reason for setting 100° as the upper limit is because that ice wedges with angles beyond this value shall violate our initial assumption and develop radial crack before the circumferential crack. Detailed reasonings and quantifications in this regard are presented in Section 4.2. In case of the interaction velocity, 11 cases are chosen in the range from 0.1 m/s to 10 m/s. The range of these physical values are determined primarily based on typical ice – structure interaction experiences. Additionally, we utilize Eq. (5) to correlate the vertical interaction velocity v_v of the structure with the 'vertical loading rate $\dot{f}_t$' on the ice wedge. The implicit assumption here is that the crushing depth δ in the vertical direction can be linearly scaled with the contact force (see Fig. 7). When the vertical crushing depth δ is small, it is true that the contact area often increases with the crushing depth, thereby leading to an increase in the contact force. Normally, during ice – sloping structure interactions, the crushing depth is much smaller than the ice thickness before bending failure takes place. Therefore, we expect that a linear scaling between the contact force and crushing depth as in Eq. (5) is a fair approximation. In addition, the influence of the in-plane compressive force is ignored in the simulation. Through some derivations, we come to Eq. (6), which relates the vertical velocity of the structure with the

vertical velocity v_v on the ice wedge. Without loosing generality, the results presented in this paper are based on the assumption of $\sigma_c = 1$ MPa and α=45°. This, in a way, introduces an 'equivalent vertical velocity (v)' as in Eq. (6). This will largely simplify Eq. (6) and we will present all the interaction velocity related terms with this equivalent vertical velocity. In practice, when using the results from this paper, one can easily scale the actual vertical velocity v_v according to Eq. (6) with known compressive strength σ_c and sloping structure angle α.

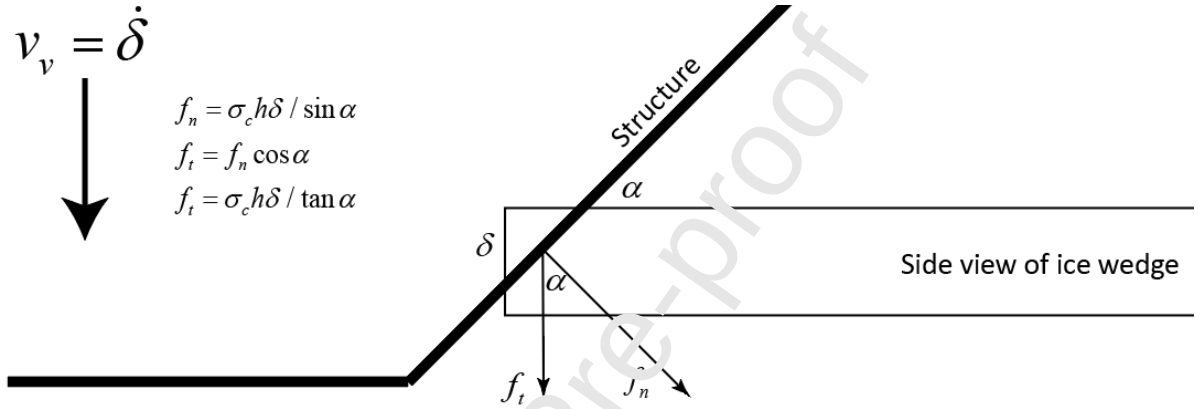

Fig. 7. Relating the interaction velocity with the applied loading rate in the simulation.

$$\frac{\delta}{\tan\alpha} = \frac{f_t}{\sigma_c h}, \text{and } \frac{v_v}{\tan\alpha} = \frac{\dot{\delta}}{\tan\alpha} = \frac{\dot{f}_t}{\sigma_c h} \quad (5)$$

$$v = \frac{v_v}{\tan\alpha} \times \frac{\sigma_c}{1\,[\text{MPa}]} \quad (6)$$

For the static cases, the interaction velocity is not considered. A total of 20 (i.e., loading radius variation) × 6 (i.e., wedge angle variation) = 120 cases are tested. On the other hands, a total of 20 × 6 × 11 (i.e., interaction velocity variation) = 1320 cases are simulated for the dynamic cases. The modeling automation is achieved by Python scripting. When all modeling were completed, all cases were run sequentially through the parametric study scripting.

Table 2 Numerical testing matrix

Parameter	Range	Unit	Number
Loading radius ($\frac{a}{l_c}$)	[0.05 ~ 1.0 with interval of 0.05]	-	20
Wedge angle	[30, 45, 60, 75, 90, 100]	°	6
Interaction velocity (v)	[0.1, 0.3, 0.5, 0.7, 1, 2, 3, 4, 6, 8, 10]	m/s	11

4. Numerical test results

Numerical test results in static and dynamic conditions are presented in this section. The static tests are carried out to check the validity of the numerical model by comparing the ice breaking force and length against known quasi-static solutions. The dynamic cases are performed to generate the data base with target values and to explore the influences of loading radiuses, wedge angles, and the interaction velocity.

4.1 Static test results

4.1.1 Comparison with existing analytical solutions

Static test results for the ice breaking force and length are presented in Fig. 8 and Fig. 9, respectively. These values are obtained by the assumption that the failure starts when the radial stress of the ice surface exceeds the ice flexural strength. Radial stresses are captured along the reference line (See Fig. 4). In Fig. 8 (a), the calculated breaking forces are normalized in the form $\frac{\pi}{\theta}\frac{3f_b}{2\sigma_f h^2}$ to compare with the adaptation of Nevel's solution (Lu et al., 2016) presented in Eq. (2). Such normalization process pre-assumes that the breaking force can be linearly scaled with the wedge angle θ. However, the simulation results are quite scattered for different wedge angles, as shown in Fig. 8 (a); and the only good agreement was found for the case with a wedge angle of 30°, which is a relatively narrow wedge. This corresponds well with the infinite narrow wedge assumption behind the original solution of (Nevel, 1958). To better adapt Nevel's narrow wedge solution to wedges with wider angles, a trial-and-error normalization procedure was conducted, and it turns out that when the ice breaking force is normalized in the form of $(\frac{\pi}{\theta})^{1.15}\frac{3f_b}{2\sigma_f h^2}$, a more converged solution is achieved in Fig. 8 (b) with a new form of equation (see Eq. (7)).

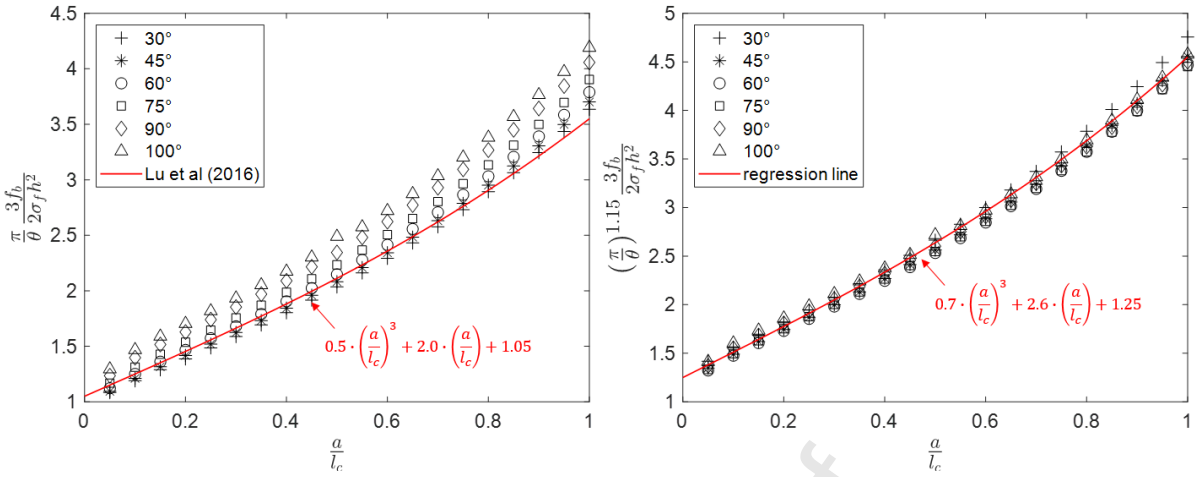

(a) Regression with Lu et al (2016) (b) Regression with the proposed equation

Fig. 8 Equation for breaking force in static condition

$$\left(\frac{\pi}{\theta}\right)^{1.15}\frac{3f_b}{2\sigma_f h^2}=0.7\left(\frac{a}{l_c}\right)^3+2.6\left(\frac{a}{l_c}\right)+1.25 \tag{7}$$

Fig. 9(a) shows the normalized breaking length $\frac{l_b}{l_c}$ versus the loading radius with varying wedge angles and compares with the data points from Nevel (1972). Unlike the breaking force, the breaking length does not seem to be significantly affected by the wedge angle, and the result shows an overall good agreement with Nevel (1972), where the wedge angle is not taken into account. In particular, Nevel (1972) seems to fit better with wedges of relatively small angle. For more accurate fitting, we brought in a factor of $\left(\frac{\pi}{\theta}\right)^{0.05}$ and normalize the ice breaking length $\frac{l_b}{l_c}$ further into $\left(\frac{\pi}{\theta}\right)^{0.05}\frac{l_b}{l_c}$. This leads to a better fitting in Fig. 9(b). Some scatters can be observed at $\frac{a}{l_c}$ = 0.05. This is because the wedge is largely affected by circumferential stress when the loading radius is small. This will be reviewed in Section 4.1.2. together with the relevant analysis results. The derived equation for the static ice breaking length is presented in Eq. (8).

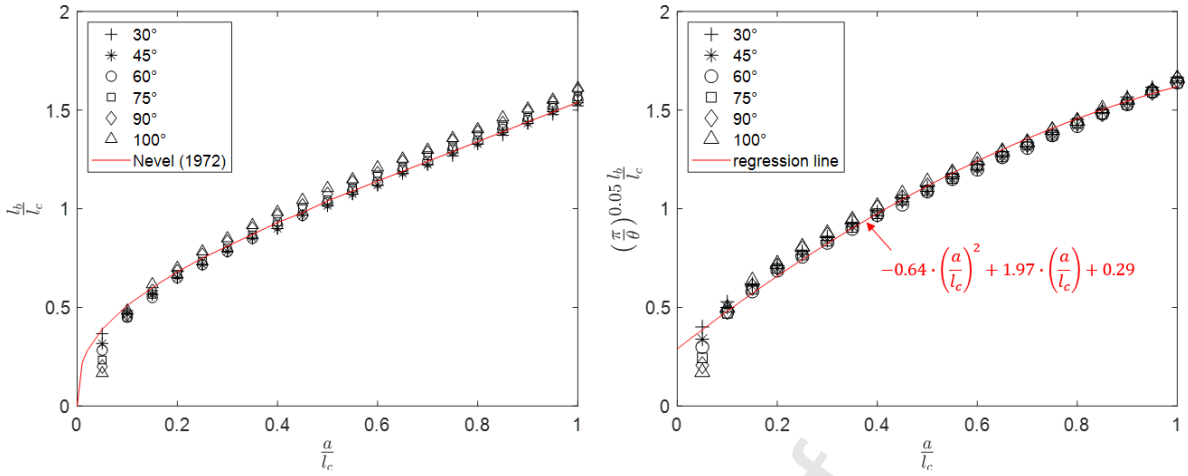

(a) Regression without angle effect (b) Regression with angle effect

Fig. 9 Equation for breaking length in static condition

$$\left(\frac{\pi}{\theta}\right)^{0.05}\frac{l_b}{l_c}=-0.64\left(\frac{a}{l_c}\right)^2+1.97\left(\frac{a}{l_c}\right)+0.29 \tag{8}$$

In so far, it is fair to conclude that we have a reasonable numerical model that agrees well with the existing static solution of Nevel (1972) in terms of both the ice breaking force and ice breaking length. However, as Nevel's solution are limited to narrow wedges, the best match is found only for rather narrow wedges (i.e., the case with 30° wedge angle among all trial simulations). Therefore, in this section, we have also extended Nevel's static solution to wider wedge angles. These are Eq. (7) for the ice breaking force with a more than linear influence from the wedge angle; and Eq. (8) for the ice breaking length with a minor influence from the wedge angle.

4.1.2 Transition from circumferential crack to radial crack

The static analysis also reveals the transition from 'circumferential crack first' to 'radial crack first' failure processes. This is examined by comparing the stress components in circumferential and radial directions with varying wedge angles and loading radiuses. The general rationale behind this examination is that: if the maximum radial stress is larger than the maximum radial stress in the simulation domain, the ice wedge will develop radial crack first. And vice versa.

Intuitively, when an ice wedge gets narrower, it is easier to develop circumferential crack first. Conversely, a radial crack tends to develop first for a wider ice wedge. For example, when the wedge angle is 180°, the problem reduces to the bending failure of a semi-infinite ice plate, in which, it is generally accepted that a radial

crack shall always develop first under a vertical load (Kerr, 1976). For the loading radius, we can also intuitively assert that when the load radius is large, i.e., $\frac{a}{l_c}$ is large, an ice wedge is easier to fail by forming circumferential cracks first. In this section, we try to quantitatively assess such 'circumferential crack first' to 'radial crack first' transition under the influence of wedge angles and loading radiuses.

First, in Fig. 10, the circumferential stress ($\sigma_{\theta\theta}$, responsible for radial cracks) and the radial stress (σ_{rr}, responsible for circumferential cracks) are presented along the reference line (See Fig. 4) with varying wedge angles. The loading radius is fixed as $\frac{a}{l_c}$ = 0.05. As expected, as the wedge angle increases, the circumferential stress keeps increasing and overtakes the radial stress when the wedge angle reaches 105°. This marks the angle (i.e., between 100° and 105°) larger than which, the radial crack develops earlier than the circumferential crack. Based on this study, we shall limit our simulated wedge angles below 100°; and derive the dynamic wedge bending formulas that are only suitable for wedges that are smaller than 100°. In practice, if an ice wedge larger than 100° is encountered, as radial cracks shall develop first, the 100° ice wedge will be intersected into several ice wedges with smaller angles where our developed formulas can be applied individually. This approach has been adopted in (Lubbad and Løset, 2011).

In Fig. 11, we presented the circumferential stress and the radial stress along the edge line similar to Fig. 10. As expected, the circumferential stress (responsible for radial crack) is negligibly small comparing to the radial stress (responsible for circumferential crack). Naturally, a radial crack is unlikely to develop at near-edge regions of an ice wedge comparing to its center. Therefore, it makes sense as in Fig. 10 to only investigate the radial and circumferential stresses at the center line of an ice wedge to study its failure pattern.

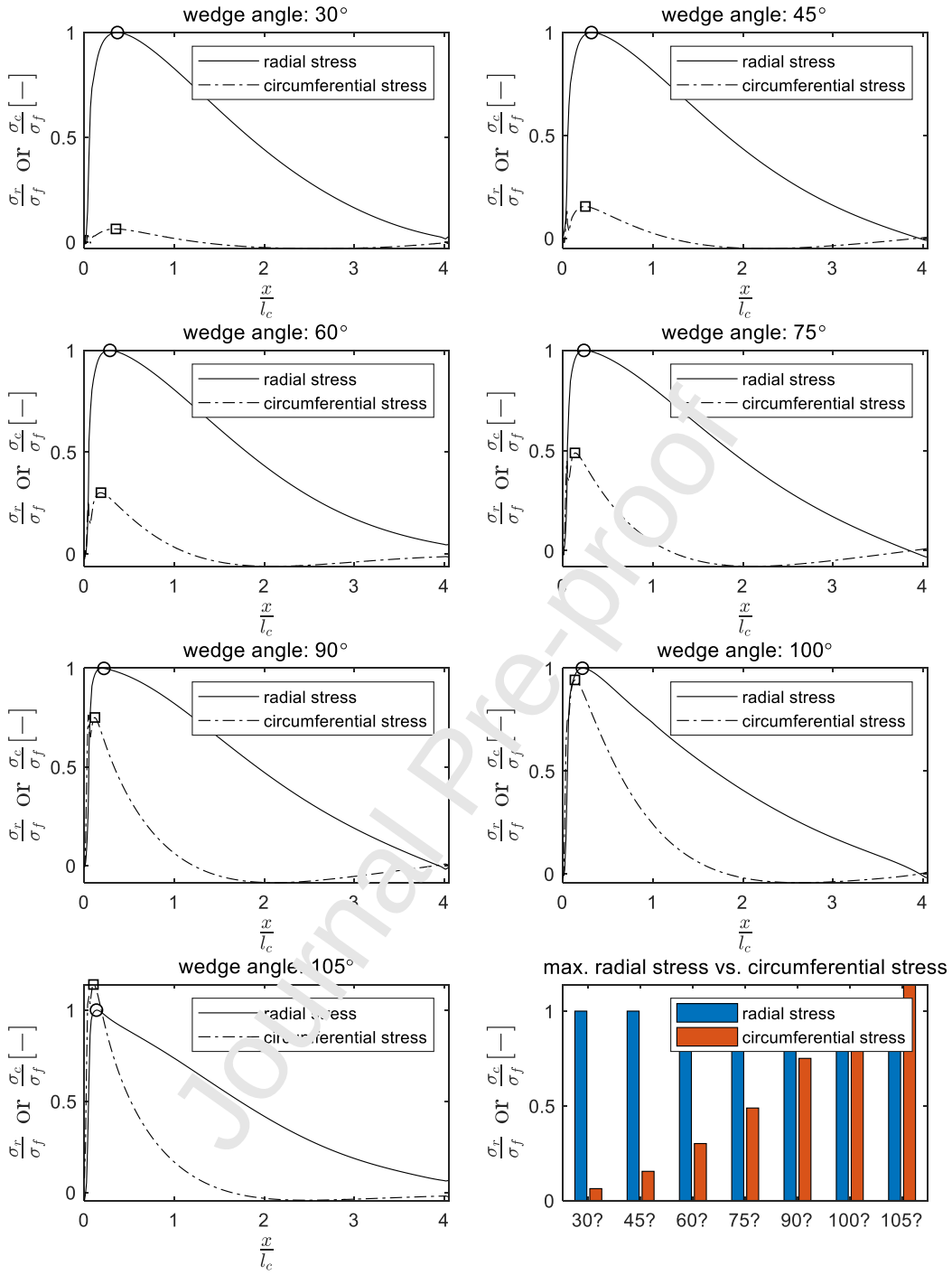

Fig. 10 Comparisons of radial stress and circumferential stress along reference line according to different wedge angles ($\boldsymbol{h}$ = 1 m, $\frac{\boldsymbol{a}}{\boldsymbol{l_c}}$ = 0.05)

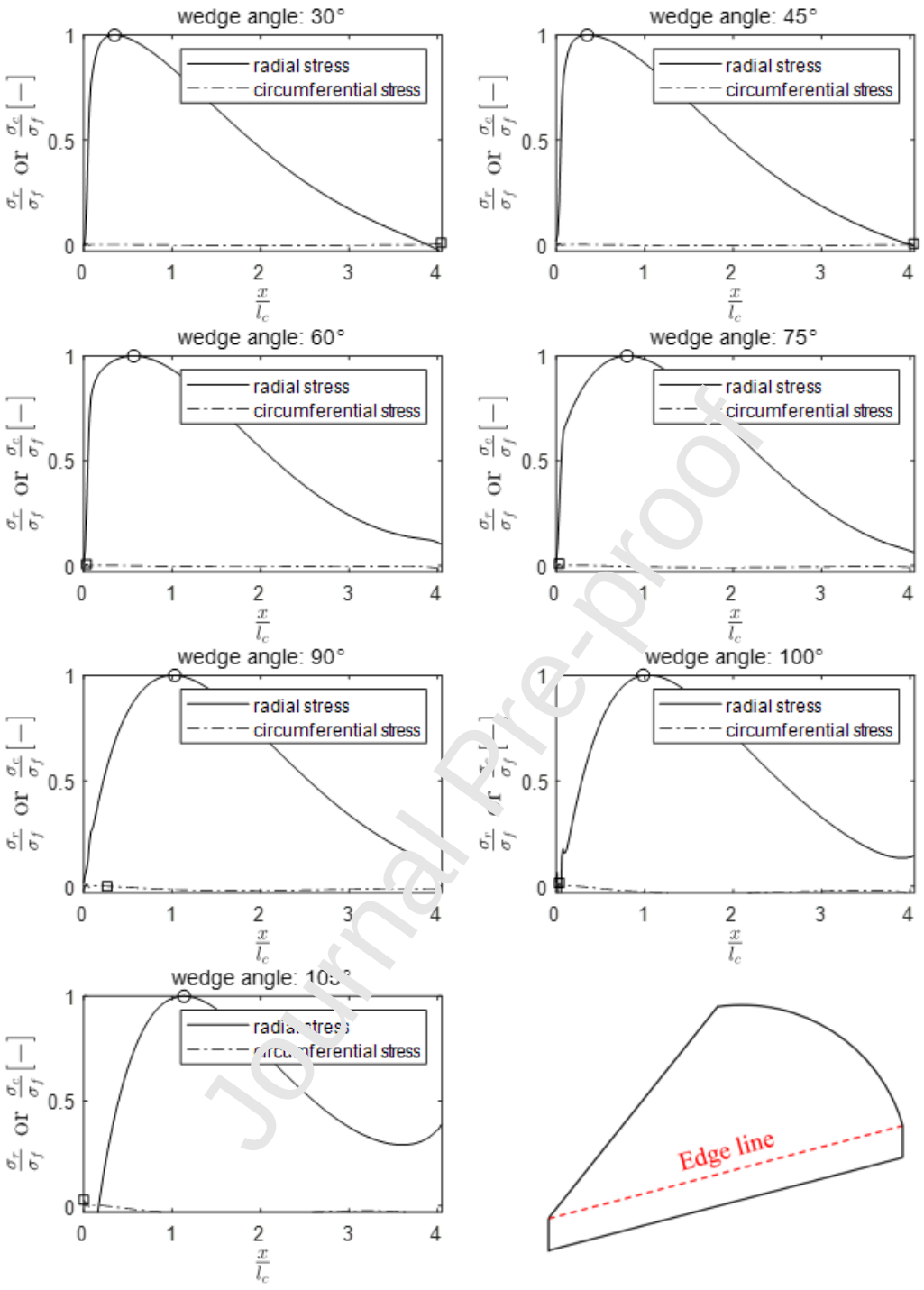

Fig. 11 Comparisons of radial stress and circumferential stress along edge line according to different wedge angles (h = 1 m, $\frac{a}{l_c}$ = 0.05)

Next, we fix the wedge angle as 100°, and compare the two stress components along the reference line with varying loading radiuses (see Fig. 12). Combining with Fig. 10, we can see that the radial stress (σ_{rr}) is not too much influenced by both the wedge angle and loading radius. From Fig. 12, we also see that the circumferential stress ($\sigma_{\theta\theta}$) decreases, expectedly, with increasing loading radius.

Based on the results from both Figs. 10 and 12, it is safe to conclude that circumferential cracks will develop first for ice wedges that are smaller than around 100°, irrespective of the loading radius that are of typical engineering relevance. This is also the reason that we set out wedge angle's simulation range within 100°.

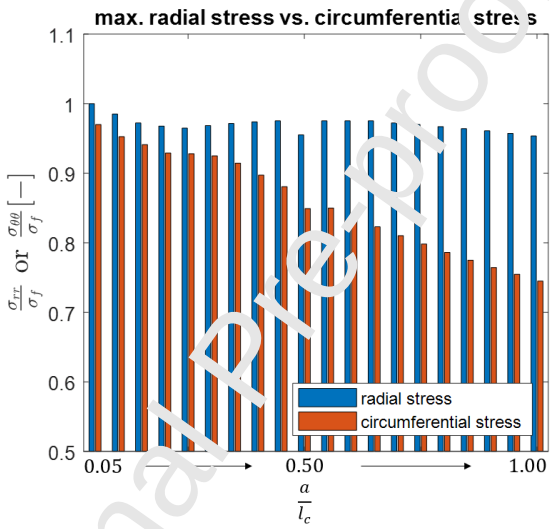

Fig. 12 Comparisons of radial stress and circumferential stress according to different loading radiuses

4.2 Dynamic test results

In this section, we examine how the breaking force and length vary with, among many factors, the presence of loading rates/velocity. Different from the static case, for visual illustrations, we explicitly simulated the post-failure process based on the implemented yielding criteria and the cohesive zone model. However, as stressed before, our interested outcomes, i.e., the ice breaking force and length are independent from the post-failure behavior. Fig. 13 illustrates a simulation example for the 45° wedge angle and $\frac{a}{l_c} = 0.05$ loading radius case. It vividly re-confirms the generally accepted trend that a faster loading rate leads to a shorter ice breaking length.

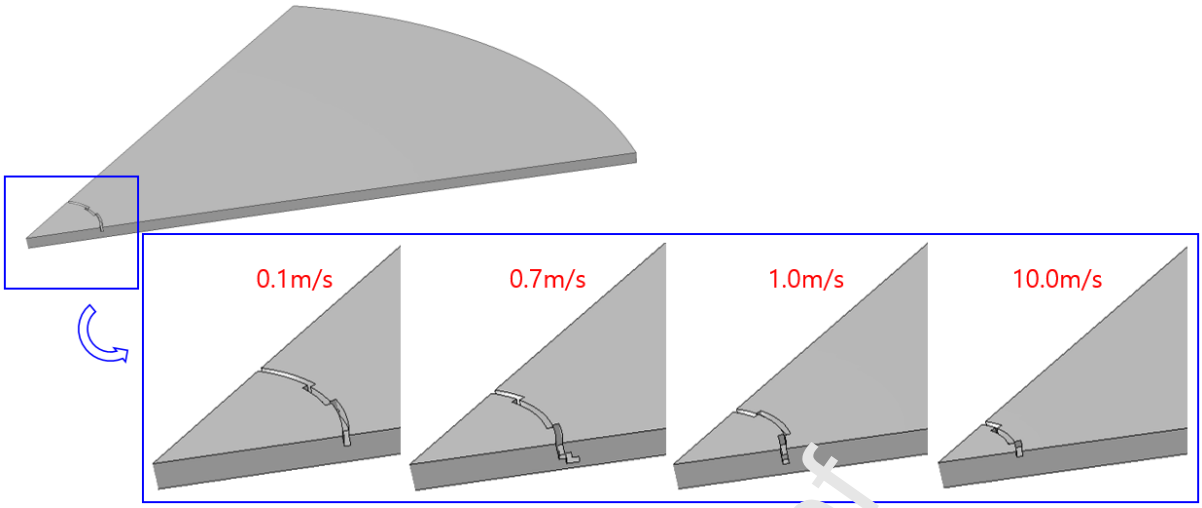

Fig. 13 Ice breaking patterns according to interaction velocity (wedge angle: 45° and loading radius $\frac{a}{l_c}$: 0.05)

Fig. 14 and Fig. 15 present the ice breaking force as a function of interaction velocity according to different wedge angles and loading radiuses, respectively. For generalization of the results, the variables applied to the analysis are normalized as follows:

$\frac{\theta}{\pi}$ is the normalized ice wedge angle;

$\frac{a}{l_c}$ is the normalized loading radius;

$\frac{v}{\sqrt{gh}}$ is the normalized interaction velocity;

$\frac{f_b}{\sigma_f h^2}$ is the normalized ice breaking force;

$\frac{l_b}{l_c}$ is the normalized ice breaking length;

For better readability, the cases with $\frac{a}{l_c}$ = 0.1, 0.5 and 1.0 are presented in Fig. 14, and cases with $\frac{a}{l_c}$ = 0.2, 0.4, 0.6 and 0.8 are separately presented in Fig. 15. It can be seen that the breaking force increases with increasing velocity, with increasing wedge angle, and increasing loading radius, i.e., these terms are positively correlated. However, it can be observed that the detailed increasing pattern according to the interaction velocity is slightly different for each wedge angle and loading radius, indicating a nonlinear influence from the wedge angle and loading radius.

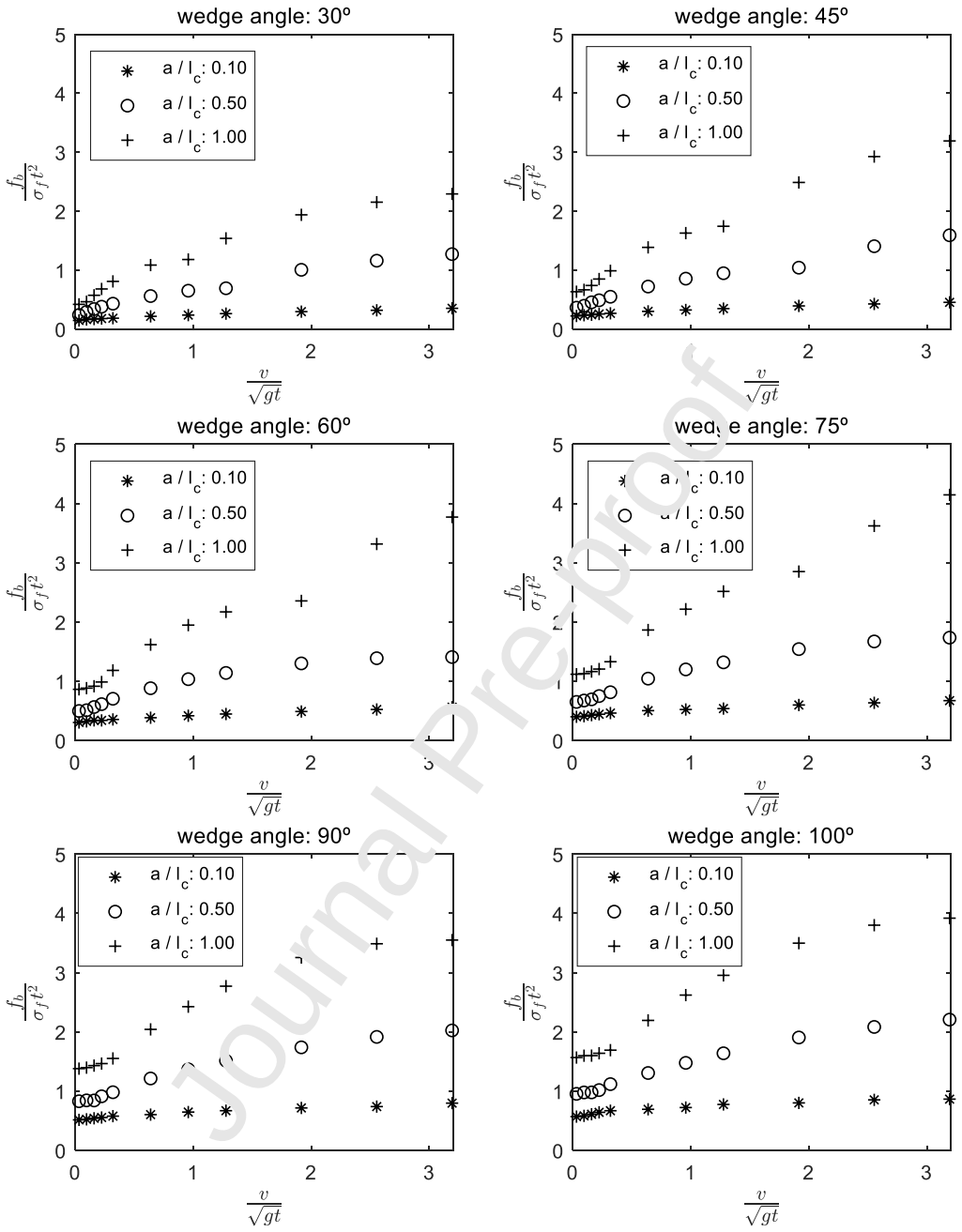

Fig. 14 Ice breaking force as a function of interaction velocity with varying wedge angles

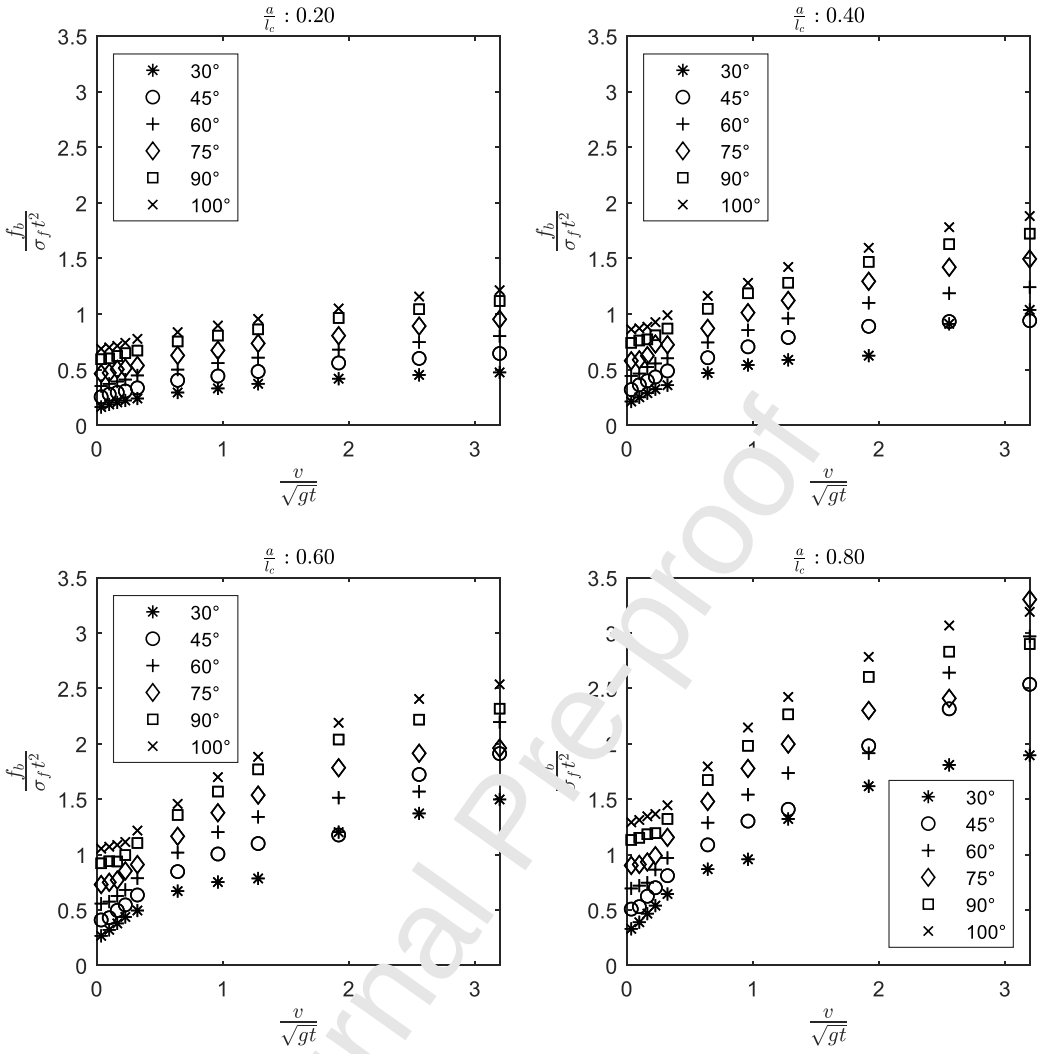

Fig. 15 Ice breaking force as a function of interaction velocity with varying loading radiuses

Fig. 16 and Fig. 17 present the ice breaking length as a function of interaction velocity according to different wedge angles and loading radiuses, respectively. Similar to the visual illustration in Fig. 13, we quantitatively show that given the same wedge angle and load radius, a faster interaction velocity/loading rates leads to a shorter the breaking length. Moreover, similar to the static cases, the breaking length increases with increasing loading radius; but is less dependent on the wedge angle.

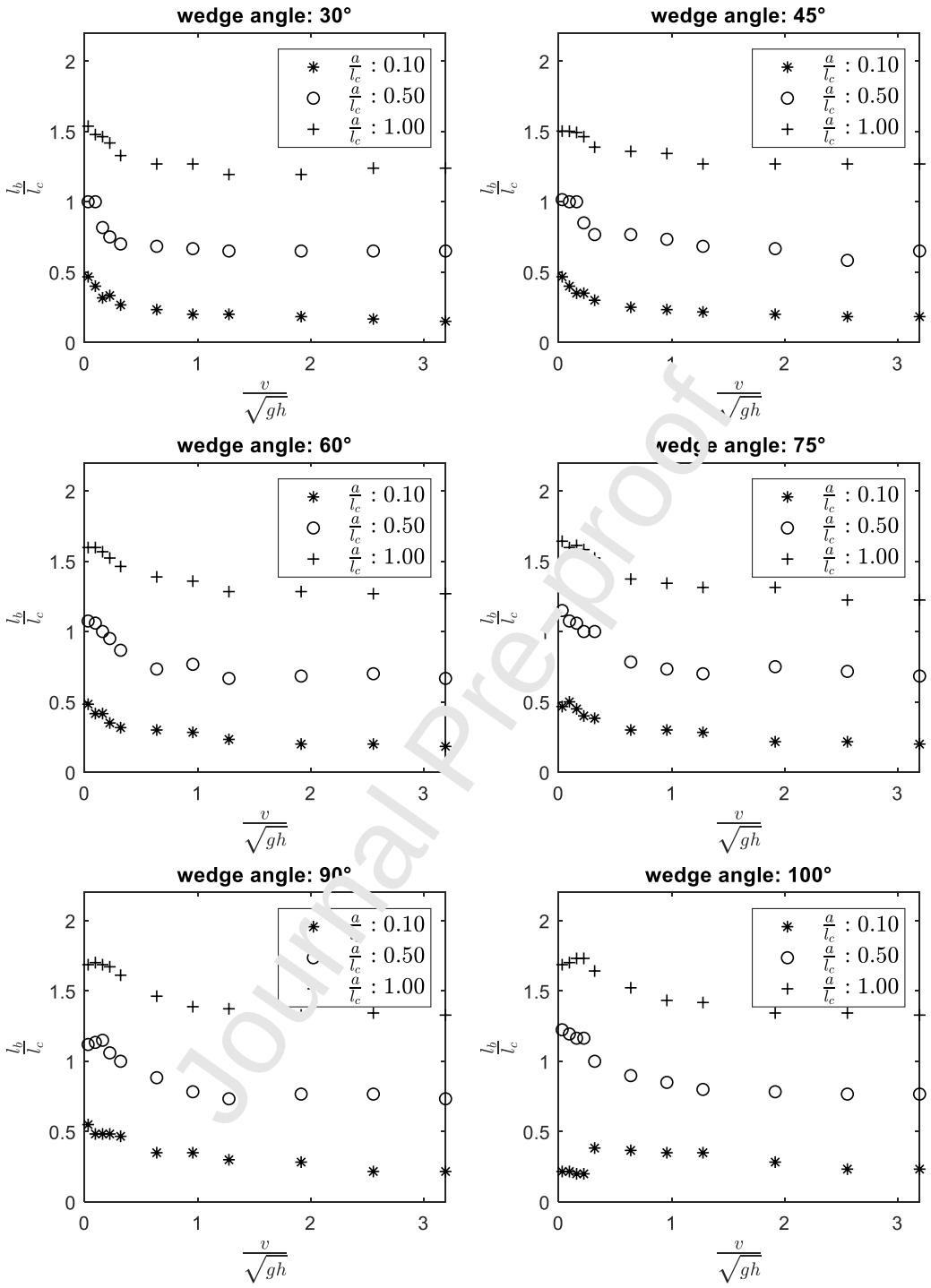

Fig. 16 Ice breaking length as a function of interaction velocity with different wedge angles.

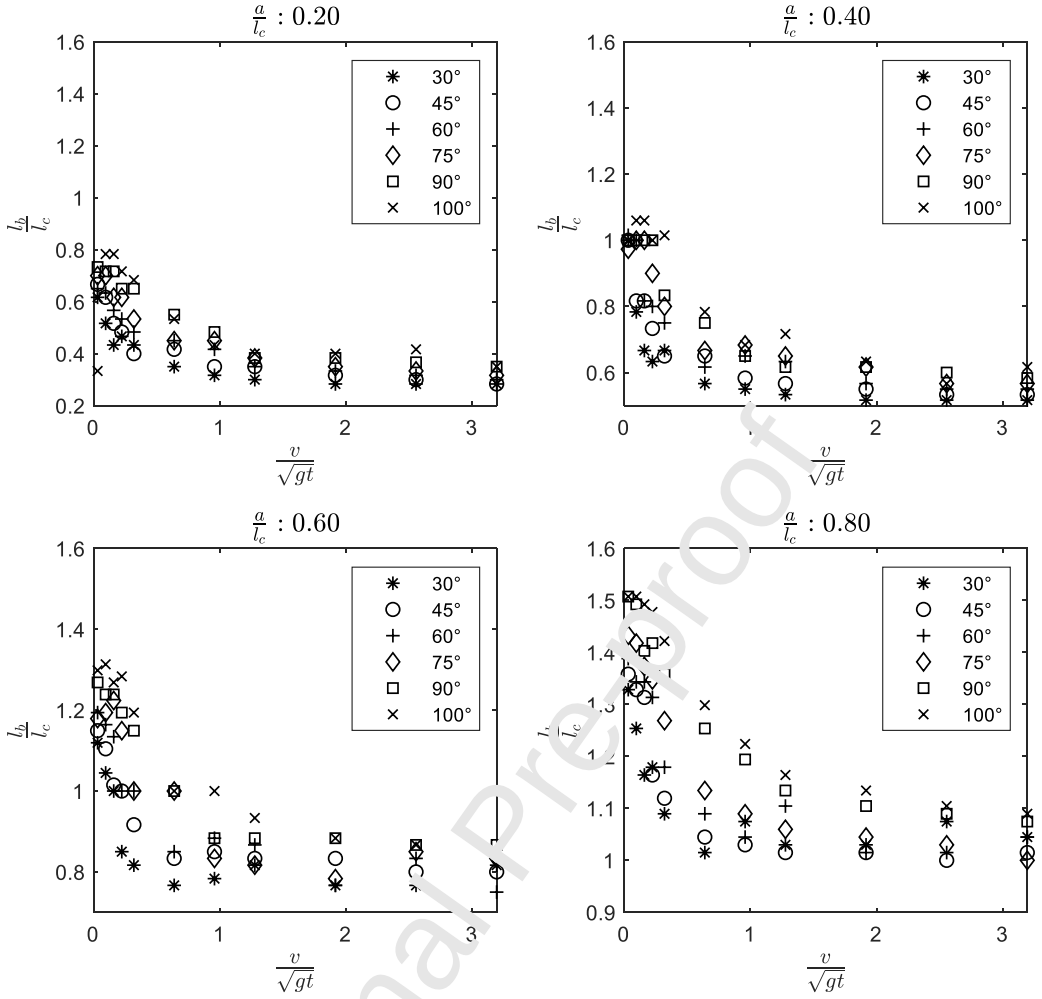

Fig. 17 Ice breaking length as a function of interaction velocity with different loading radiuses (note that the ice breaking length is less dependent on or less sensitive to the wedge angle).

5. Prediction model

The results presented in Section 4, especially the dynamic results, demonstrate the nonlinear relationship between the outputs (i.e., ice breaking force and length) and the inputs (i.e., varying interaction velocity, loading radius and wedge angles). In situations as such, the presented ANN technique suits perfectly in developing a closed-form equation based on the available inputs and outputs. This section presents the detailed model structure and optimization process for the development of the ANN model and the final equation.

5.1 ANN model structure

The structure of the ANN model applied in this study is shown in Fig. 18. It is a typical three-layer perceptron neural network model composed of an input layer, a hidden layer and an output layer. Each layer consists of neurons. The number of neurons in the input layer and the output layer is same with the number of inputs and the outputs, respectively. The number of neurons in the hidden layer can be determined in a variety of ways (Masters, 1993; Stathakis, 2009). In this study, its number was determined based on the results of a case study conducted on several cases selected through related theories (See Section 5.2).

The input layer has the input vector $\{P\}$ of a given length. In this application, we have three inputs (i.e., ice wedge angle, loading radius and interaction velocity) and the size of $\{P\}$ is 3×1. The hidden layer takes $\{P\}$, and it is multiplied by a weight matrix $[U]$, whose size is determined by the number of inputs and hidden layer neurons; then it adds a bias vector $\{b\}$. In the hidden layer, the derived vector $[U]\{P\}+\{b\}$ goes through the nonlinear activation function for a nonlinear mapping between inputs and outputs. The hyperbolic tangent function, which is the most commonly used function in the multi-layer perceptron model, is used as the nonlinear activation function in this study because of its fast convergence. When the vector $[U]\{P\}+\{b\}$ passes the hyperbolic tangent function, all values are transformed to a region between -1 and 1.To take this into account, all input data are normalized between -1 and 1 before training. The normalization is important for the efficiency and accuracy of the system as it treats all variables equally. Eq. (9) is utilized to normalize the input variables. The activated vector enters the output layer, in which, a bias vector, $\{s\}$ is added to derive the output vector $\{y\}$. In this application, we aim to output two variables, i.e., the ice breaking force and length; thus $\{y\}$ is a 2×1 vector.

The whole calculation process is expressed in vector notations as presented in Eq. (10). In the end, the output vector can be de-normalized to the original input range.

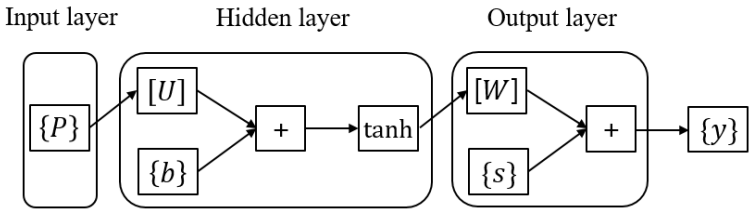

Fig. 18 Structure of the ANN model in this study

$$X_N = 2 \times \left[\frac{X_R - X_{min}}{X_{max} - X_{min}}\right] - 1 \quad (9)$$

in which,

X_N is the normalized value;

X_R is the original value;

X_{min} is the minimum value of X_R;

X_{max} is the maximum value of X_R;

$$\{y\} = \{s\} + [W]^T \tanh([U]\{P\} + \{b\}) \quad (10)$$

5.2 ANN model optimization

The effectiveness and accuracy of ANN models are influenced by ANN parameters such as the number of neurons in hidden layers and data splitting ratio. This section addresses the determination of ANN parameters for the model optimization.

The number of neurons in hidden layers determines the size of $[U]$, $[W]$, and $\{b\}$ in Eq. (10), i.e. $[U]$ is $N_{nh} \times N_i$ matrix, $[W]$ is $N_{nh} \times N_o$ matrix, and $\{b\}$ is a vector whose size equals to N_{nh}, where, N_{nh} is the number of neurons in hidden layer. N_i and N_o are the number of inputs and outputs, respectively. In this application, $N_i = 3$ and $N_o = 2$. If the model has a large number of neurons in the hidden layer, it becomes complicated, and the training time increases accordingly. Also, it can cause overfitting problems because a large number of neurons in the hidden layer increases the nonlinearity of the model. On the other hand, if the number is too small, a proper fitting is not possible, which affects the accuracy of the model. In many existing ANN models, the number of neurons in hidden layers has been selected between the number of inputs and outputs (Nadui et al., 2020). In this study, a case study has been performed to determine the number of neurons optimized for the simulation results as shown in Fig. 19. Since there are three inputs and two outputs (i.e., $N_i = 3$ and $N_o = 2$), we calculated the performances according to the number of neurons within the range from two to six. Here, two different

indicators are employed to assess the model performance. These are the 'Pearson correlation coefficient' (defined in Eq. (11)) and the 'index of agreement' (defined in Eq. (12)). The Pearson correlation coefficient (ρ_{xy}) can be used to quantify the linear relationship between two variables, e.g., *x* and *y*. A larger absolute value $|\rho_{xy}|$ represents a stronger dependence between x and y. In addition, the index of agreement (I) has been further employed to evaluate the performance of the model in terms of the prediction error. The index of agreement represents the ratio of the mean squared error and the potential error given in Eq. (12). The results in Fig. 19 show that: the six neurons case shows the highest performance in the Pearson correlation coefficient, and the five neurons case shows the highest performance in the index of agreement. In general, all the performances are rather good with a value of around 99.5%. Given this assessment, in this application, the five neuron - case is chosen in the hidden layer. After determining the number of neurons, we also need to investigate the data splitting ratio in constructing an efficient and accurate ANN model.

$$\rho_{xy} = \frac{Cov(x,y)}{\sigma_x \sigma_y} \tag{11}$$

in which,

$Cov(x, y)$ is the covariance of variables x and y,

σ_x and σ_y are the standard deviation of x and y;

$$I = 1 - \frac{\sum_{i=1}^{N}(y_i - \hat{y}_i)^2}{\sum_{i=1}^{N}(|y_i - \bar{\hat{y}}| + |\hat{y}_i - \bar{\hat{y}}|)^2} \tag{12}$$

in which,

N is the number of samples;

y_i is the predicted value;

$\hat{y}_i$ is the target value;

$\bar{\hat{y}}$ is the average of the target values.

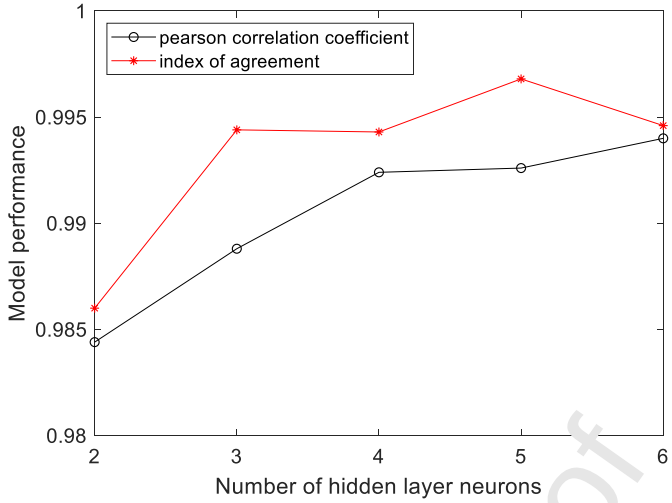

Fig. 19 Model performance according to the number of hidden-layer neurons

In general, the dataset to be used for ANN is randomly divided into three subsets, i.e. training, validation and testing datasets with a certain ratio to avoid the typical problem of overfitting. Firstly, the coefficients of the ANN model such as weights and biases are derived based on the training dataset. Then the performance of the fitted ANN model is evaluated using the validation dataset, and the coefficients are tuned to increase the ability to generalize. Finally, the goodness of fitting of the model is evaluated by the performance test based on the test dataset.

To find a splitting ratio optimized for the data prepared in this study, a sensitivity study is performed on commonly used splitting ratios, which are '60% / 20% / 20%', '70% / 15% / 15%' and '70% / 20% / 10%' for training, validation and testing, respectively. Performances based on the Pearson correlation coefficient for each model with different splitting ratio are evaluated as shown in Fig. 20. It shows that the ratio of, '70% / 15% / 15%' case gives the most consistent results. In case of '70% / 20% / 10%', the model performance shows a relatively larger fluctuation because it depends largely on the selected data when the number of test data is small. Therefore, the '70% / 15% / 15%' is chosen as the data splitting ratio in this study.

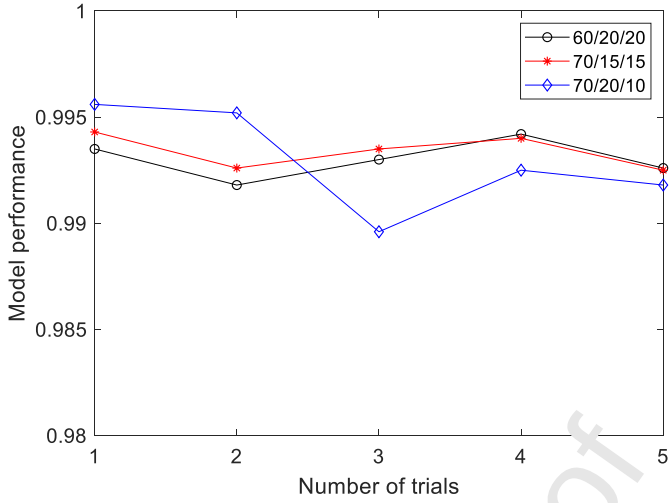

Fig. 20 Model performance according to different splitting ratio

5.3 Final ANN model

Based on the basic structure and the optimization process described in Sections 5.1 and 5.2, an ANN model is developed to predict the ice breaking force and the corresponding ice breaking length. Despite that we have also generated results for the cases with a wedge angle of 100°, they are not included in developing the ANN model. This is because the 100° to 105° wedge angle range most likely marks the transition of failure patterns as explained in Section 4.2. Since this paper focuses only on the circumferential crack controlled wedge bending and to achieve more consistent results and model fitting, we limit the application of the model to up to 90°. Table 3 shows the maximum and minimum values to be used for normalization and denormalization of the model.

Table 3 Min. and max. values of the inputs for normalization and denormalization

Input	Min. value	Max. value	Remark
$\frac{\theta}{\pi}$	0.1667	0.5	Wedge angle
$\frac{a}{l_c}$	0.05	1	Loading radius
$\frac{v}{\sqrt{gh}}$	0.0319	3.1928	Velocity
$\frac{f_b}{\sigma_f h^2}$	0.1329	4.1447	Breaking force

$\frac{l_b}{l_c}$	0.1	1.7015	Breaking length

Substituting the normalized inputs into Eq. (13), we can calculate the normalized outputs and get the ice breaking force and length by de-normalizing the results using Eq. (9). In Eq. (13), $(-)_N$ represents the normalized value.

$$\{y\} = \{s\} + [W]^T tanh([U]\{P\} + \{b\}) \tag{13}$$

$$\{y\} = \begin{Bmatrix} \left(\frac{f_b}{\sigma_f h^2}\right)_N \\ \left(\frac{l_b}{l_c}\right)_N \end{Bmatrix}, \quad \{s\} = \begin{Bmatrix} 0.44168 \\ -0.44323 \end{Bmatrix}, \quad [W] = \begin{bmatrix} -0.62279 & 1.11512 \\ 1.43578 & 0.75029 \\ 1.19394 & 0.16605 \\ 1.30548 & 0.88875 \\ 0.11579 & -0.32836 \end{bmatrix},$$

$$[U] = \begin{bmatrix} 0.08632 & 0.41875 & 0.20475 \\ 0.13452 & 0.41314 & 0.35316 \\ 0.2035 & -0.20983 & 0.49023 \\ -0.09635 & 0.44944 & -0.44704 \\ -0.27187 & -0.55681 & 3.54993 \end{bmatrix}, \quad \{P\} = \begin{Bmatrix} \left(\frac{\theta}{\pi}\right)_N \\ \left(\frac{a}{l_c}\right)_N \\ \left(\frac{1}{\sqrt{g}}\right)_N \end{Bmatrix}, \quad \{b\} = \begin{Bmatrix} 1.01536 \\ -0.83772 \\ 0.13003 \\ 0.24786 \\ 3.30743 \end{Bmatrix}$$

6. Validation of the ANN model

The ANN model (Eq. (13)) developed in this study is validated in three different ways. Firstly, it is compared with the FEM data used for model development. Despite the ANN model is developed from the same FEM simulation data; this comparison can show how well the final model fits the original input data. Secondly, the ANN model prediction is compared with available existing numerical results, i.e., Sawamura et al. (2010) performed numerical simulations on the ice wedge breaking considering its dynamic effect using an Lagrangian mesh and a penalty contact algorithm. Finally, the ANN model prediction is compared with existing field data on the breaking length reported in several early researches and summarized by Naegle (1980).

6.1 Comparison with FEM data

In Fig. 21, the ANN predicted values (surface) and FEM data (red circle) in terms of the ice breaking force are presented in 3D plots. It shows a good overall agreement; but a slight deviation occurs at high interaction

velocities. More details on the deviation will be discussed in Section 7.

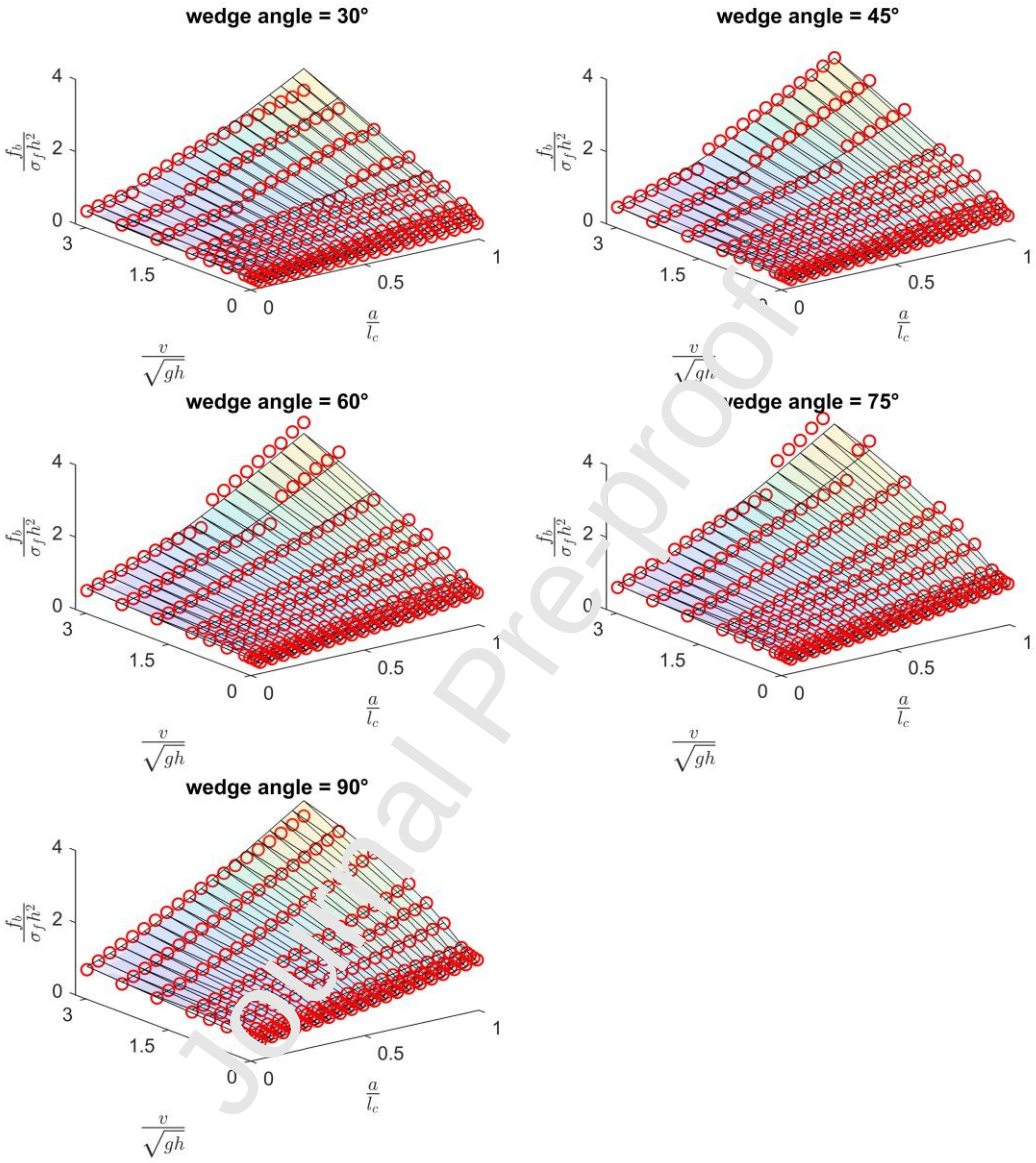

Fig. 21 Comparison of ice breaking forces from the ANN model and target FEM simulated values.

A same comparison of ice breaking length is presented in Fig. 22. Similar to the breaking force results, Fig. 22 shows good agreement overall. However, there is a relatively large deviation for the cases with a large wedge angle and a small loading radius. In particular, we can see a large discrepancy in the case with a wedge angle of 90° and with a loading radius of $\frac{a}{l_c}$ = 0.05. This is again speculated to be caused by the failure pattern

transition. Given this result, the application of the ANN model at $\frac{a}{l_c}$ = 0.05 condition is not recommended.

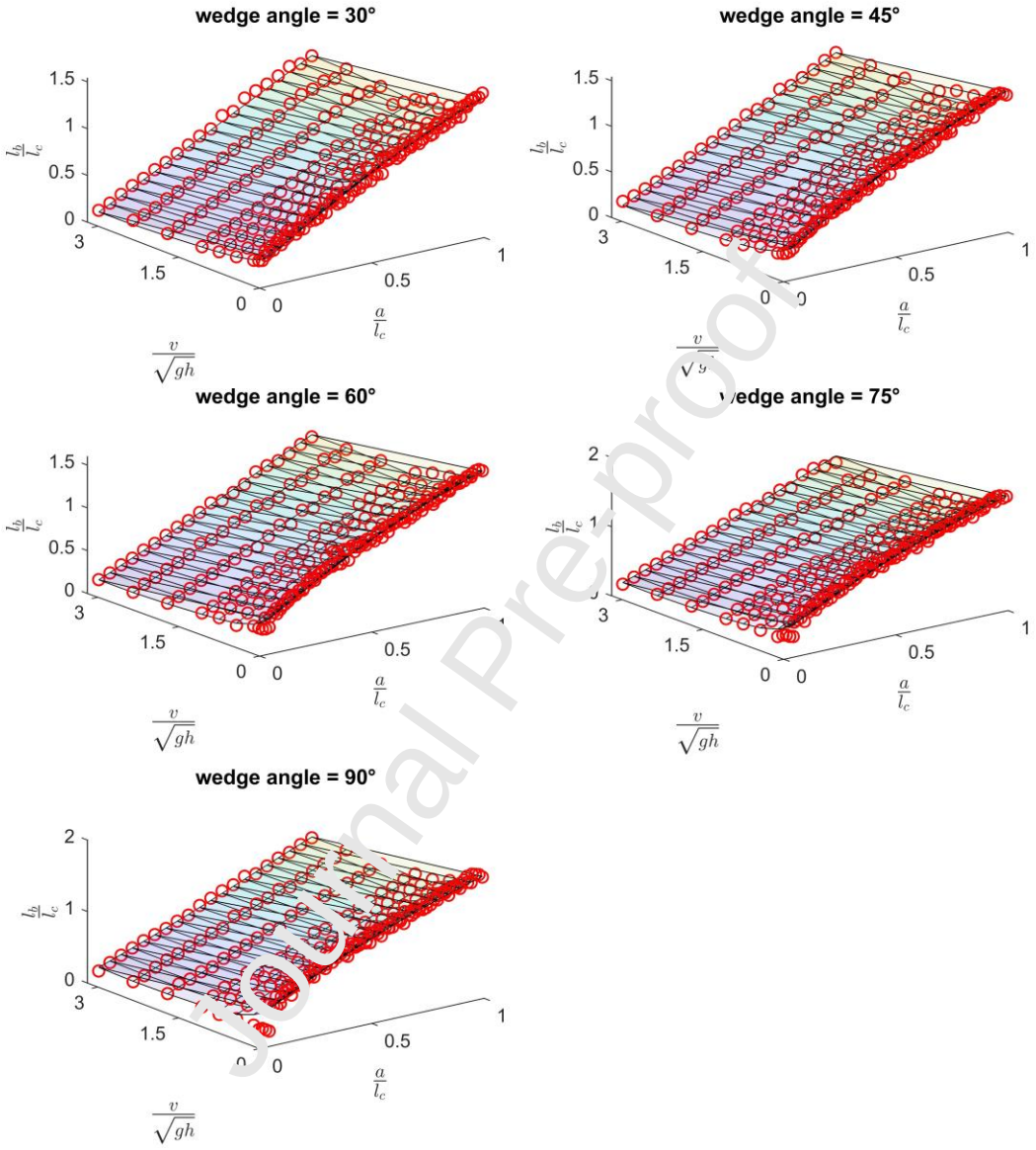

Fig. 22 Comparison of ice breaking length between ANN model and target FEM simulated values.

6.2 Comparison with Sawamura's results

In this section, we will compare our ANN model's prediction with relevant results obtained by Sawamura (2010). However, it is important to firstly point out that there are three differences between these two results/models. The first difference is a minor one: Sawamura's results are obtained from FEM analysis of a linear-elastic ice wedge model that assumes ice failure occurs when the tensile stress at the upper surface reaches the flexural

strength. Our ANN model is based on the simulation results from the FEM model, in which, ice failure occurs when the combined stress reaches the yield surface together with a minimal amount (i.e., 30% of elastic strain) of perfectly plastic strain. When it comes to the peak force that leads to fracture initiation, these two criteria are expected to yield almost the same results as circumferential crack is crack initiation controlled. The second difference is a major one. In the simulation model of Sawamura et al. (2010), they also considered and implemented the fluid foundation as an incompressible inviscid material, in which, the hydrodynamic effects are present; whereas in our FEM model, the fluid foundation is simplified as a Winkler foundation. The third difference is that Sawamura et al. (2010) applied a point load at the vertices of the ice wedge whereas in our case we varied the loading radius. Given the premises of this comparison, we will present the comparisons in terms of the ice breaking force and ice breaking length respectively for mutually available data.

However, to make the results comparable, we first need to perform some linear transformations as similar results from both studies are presented in different coordinate systems and with different normalizations. These trivial manipulations are summarized here: 1) our interaction velocity v is converted to loading rate using Eq. (6), where the compressive strength σ_c is assumed to be 2.8 MPa (Sawamura et al, 2009); 2) the original ice breaking force results from Sawamura et al. (2010) were presented in the normal direction of the hull (i.e., f_n in Fig. 7). To make the results comparable with ours, all Sawamura's results (in terms of peak force) are converted to the vertical direction (i.e., the direction of f_t in Fig. 7).

The ice breaking forces are compared in two plots. In Fig. 23(a), various thicknesses were considered for wedge angles of 45° and 90°. In Fig. 23(b) various wedge angles were taken into account for the 1-m thick wedge. A good overall agreement is achieved. However, Sawamura et al.'s results seem to have less velocity effect than do the ANN model predictions. It should be noted that some differences in comparison are inevitable because the simulation methods used for the studies are not exactly the same. The major differences are summarized in Table 4.

Table 4 Modeling difference between Sawamura et al. (2010) and ANN model

	Sawamura et al. (2010)	ANN model
Loading radius $(\frac{a}{l_c})$	0 (point load)	0.05
Fluid foundation	Incompressible inviscid flow	Winkler-type elastic foundation

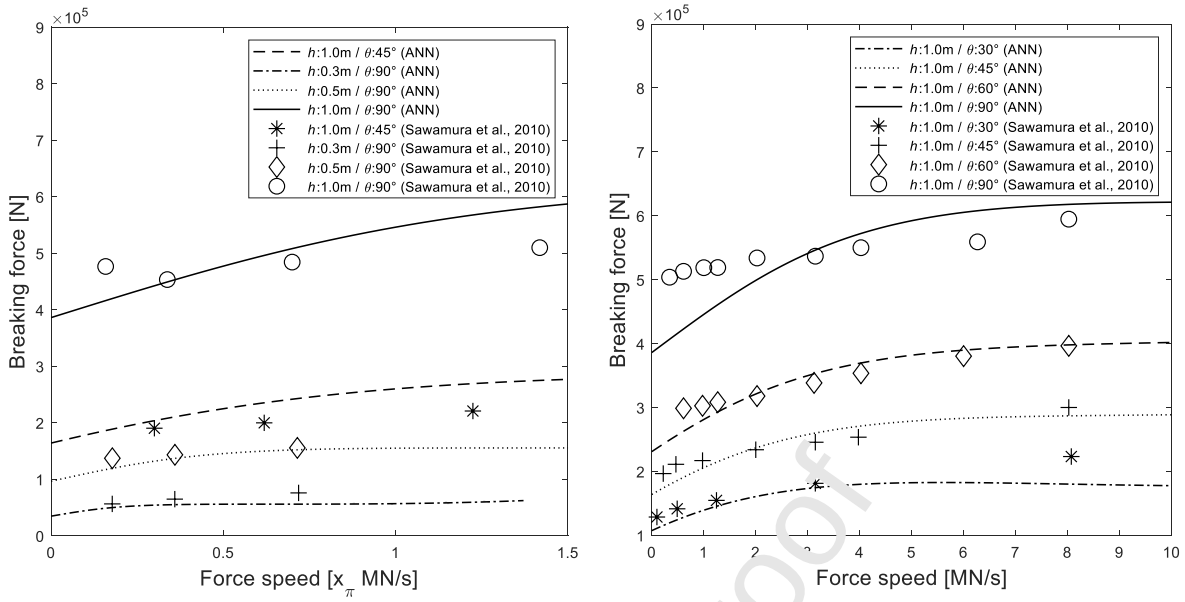

(a) Various thickness cases for wedge angles of 45° and 90° (b) Various wedge angle cases for 1 m thickness

Fig. 23 Comparison of ice breaking forces by ANN model (Eq. (13)) and Sawamura et al. (2010)

Fig. 24 compares the ice breaking lengths for various thicknesses with the wedge angles of 45° and 90° from both studies. Overall, the two results are in good agreement, except for the low velocity case with a wedge angle of 90°. In particular, in case of Sawamura et al.'s simulation, since the force was applied as point load, it is believed that the wedge failure pattern is more significantly affected by the circumferential stress at a low velocity with a wedge angle of 90°.

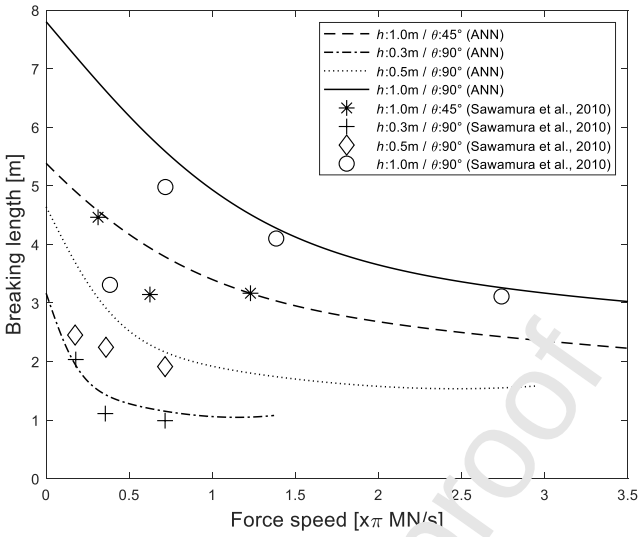

Fig. 24 Comparison of ice breaking lengths by ANN model and Sawamura et al. (2010)

6.3 Comparison with existing experimental data

The predictions by the ANN model and the existing experimental data summarized by Naegle (1980) are compared in Fig. 25. Naegle (1980) presented the experimental data on the breaking length performed by several early researchers. Since there is no information on the loading radius, the loading radius that fits the data well was varied according to experience. As a result, $\frac{a}{l_c}$ = 0.1 seems to give a good fit the overall field data. Additionally, we present two additional upper and lower predictions of the ANN model using the loading radius of $\frac{a}{l_c}$ = 0.05 and 0.15. Although Naegle's experimental results show a lot of scatter, it seems that the overall prediction and the general trend with regard to the ice breaking lengths' velocity dependence can be well captured by the ANN model.

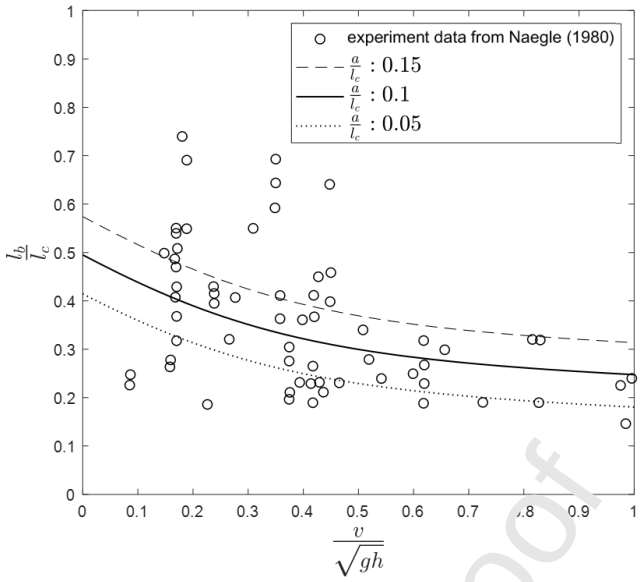

Fig. 25 Comparison of ice breaking lengths by ANN model and Naegle (1980)

7. Discussions

7.1 Influence of wedge angle, loading radius and interaction velocity on ice breaking force and length

Despite that the general trend with regard to the influences from these parameters are well known, this paper offers a more quantitative description of these parameters' influence.

From the static simulation results, the influence of the wedge angle and loading radius on the ice breaking force and length are presented in Figs. 8 and 9. The quantitative relationships are presented in Eqs. (7) and (8). Based on the simulations and data fitting, it turns out that the breaking force is scaled with $(\frac{\pi}{\theta})^{1.15}$ instead of $\frac{\pi}{\theta}$. This differs from Nevel's assumption of treating the failure of an ice sheet as the linear summation of infinite narrow wedges (Nevel, 1958). The nonlinear relationship between f_b and θ as illustrated in Figs. 8 and 9 quantitatively exposes some theoretical (but not necessarily practical) limitations in Nevel's assumption (1958). The better fitting in Fig. 8 can be equivalently translated as $f_b \propto \theta^{1.15}$, indicating a stronger (than linear) influence from the wedge angle θ on the peak force f_b. There can be many reasons behind this stronger wedge angle effect. For example, the crack closure/dome effects as studied by (Dempsey et al., 1995, Dempsey et al., 1998, Bažant and Li, 1993) can potentially/partially explain this stronger wedge angle effect. Although the crack closure phenomenon is not explicitly modelled in our FEM simulations, its physical essence that wedge materials in the circumferential direction lend support to each other, thereby increasing the overall bearing

capacity of a wider wedge is reflected by our 'intact' FEM wedge.

For the ice breaking length, Nevel's solution (for very narrow wedges) seems to give a good prediction also for wider wedges (see Fig. 9(a)). However, a better fitting can be achieved in Fig. 9(b) if we introduce a minor influence of the wedge angle, i.e., $l_b/l_c \propto \theta^{0.05}$. In comparison, there is a less profound effect from the wedge angle on the ice breaking length than on the ice breaking force.

Given the satisfactory comparisons and expected discrepancies between our numerical simulation results and the existing Nevel's quasi-static solutions, we moved on to calculate the dynamic effects on the ice wedge bending problem. Naturally, we managed to reproduce the generally accepted qualitative results that an increasing interaction velocity/loading rate leads to a larger ice breaking force and a shorter ice breaking length. Moreover, observing Figs. 14 and 15, we see that the static trends (i.e., the ice breaking force increases with increasing wedge angle and/or increasing loading radius) are magnified by the presence of faster loading rates. On the other hand, the ice breaking length tends to stabilize to certain value for each of the simulated cases (with varying wedge angles and loading radiuses) when the loading rate exceeds certain threshold, see Figs. 16 and 17. These quantitative results are generalized into a closed form equation (i.e., Eq. (13)) in this paper following the ANN model development.

7.2 Advantage of ANN

As stated in Section 7.1, the influences of wedge angle, loading radius, and interaction velocity on ice breaking force and length are nonlinear. In this case, the traditional regression method has a limitation on the form of the equation that can be created. On the other hands, ANN is a very suitable method for multivariate and nonlinear problem because numerous neurons can be trained with high degrees of freedom through iterations. Therefore, it is possible to develop a prediction model with a high accuracy regardless of the complexities of data. Moreover, its simple basic structure enables us to build a straightforward 'analytical' model expressed in matrix and vector forms. When the model is enriched with more data, the structure of the equation will not change. Therefore, it is rather efficient comparing to other methods.

In this paper, the physical complexities with regard to the influences of ice wedge angle, loading radius and loading rate (in a form of force velocity) are characterized by the developed ANN model (Eq. (13)), which is also one of the major contributions from this paper. Because of the simplicity of Eq. (13), fast calculations can be easily achieved given different ice wedge bending scenarios.

7.3 Disadvantage of ANN

Despite the simplicity and versatility of the ANN model developed in this paper (i.e., Eq. (13)), we should always have a good understanding of the advantages and disadvantages of the ANN method, based on which, Eq.(13) is derived. The ANN method is data-driven, so it is important to know what kind of data has been used for the model development, i.e., whether the amount of the data is sufficient, and how reliable the data is. If the data is of low quality or insufficient to describe the involved physics, the results derived from the model are also unreliable. In this study, the ANN model is based on the FEM simulations that are described in Section 2. The FEM model simplified the fluid foundation as a Winkler type foundation. Therefore, the hydrodynamic effects from the fluid foundation is absent in the FEM results and thereby absent from Eq. (13). In addition, the applicability of the model is limited by the range of data based on which it was developed. In other words, it cannot be used where it exceeds the range of data used for model development. In this study, we limit our model to characterize the 'circumferential crack first' ice wedge failure patterns. After extensive numerical probes, we limit our input data range as: 1) the ice wedge angle is smaller than 100°; and 2) the loading radius $\frac{a}{l_c} > 0.05$. These input data's range also limits the applicability of the ANN model. More on the applicability of our developed model shall be discussed in Section 7.4.

7.4 How to use the equations

For application purpose, we describe the usage of Eq. (13) in this section. Firstly, one needs to prepare the inputs to normalized values (i.e., $\frac{\theta}{\pi}$, $\frac{a}{l_c}$, $\frac{v}{\sqrt{gh}}$). These normalised input values should be checked with reference to the minimum and maximum values listed in Table 3. Notably, the velocity term used in Eq. (13) is the 'equivalent vertical velocity', which further depends on the compressive strength and sloping angle (see Eq. (6)). One needs to correlate the actual interaction velocity with the equivalent vertical velocity 'v' first before the normalisation procedure (i.e., $\frac{v}{\sqrt{gh}}$). Afterwards, Eq. (13) can be used to calculate the normalised ice breaking force and ice breaking length, which can then be denormalized back to the original scale i.e., f_b and l_b. Here, it should be noted that only values between the minimum and maximum values are considered valid. In constructing the ANN model (Eq.(13)), we have chosen the minimum and maximum in such a way that it fits most engineering applications with regard to ice – structure interactions. For example, assuming an ice wedge bending problem with the following typical parameters: ρ_w = 1025 kg/m^3, ζ = 0.3, h = 1 m, σ_f = 500 kPa, σ_c = 1 MPa, $\alpha = 45°$, E = 3.5 GPa, the range of the inputs and outputs are illustrated in Table 5.

Table 5 An example showing the applicable range of Eq. (13) with the typical inputs of: $\boldsymbol{\rho_w}$ = 1025 kg/m^3, $\boldsymbol{\zeta}$ = 0.3, $\boldsymbol{h}$ = 1 m, $\boldsymbol{\sigma_f}$ = 500 kPa, $\boldsymbol{E}$ = 3.5 GPa

Input	Min. value	Max. value	Remark
θ	$\frac{\pi}{6}$	$\frac{\pi}{2}$	Wedge angle
a	0.67 m	13.36 m	Loading radius of the contact area
v	0.1 m/s	10 m/s	Equivalent velocity
f_b	0.07 MN	2.07 MN	Ice breaking force
l_b	1.34 m	22.74 m	Ice breaking length

Comparing the numbers in Table 5 with an actual engineering case with the icebreaker Otso, Frej and Oden in Fig. 26(a) (taken from (Johansson and Liljestrom, 1980)) we see that for the case with the ice thickness $h = 1$ m, all three ice breakers' full transit speeds vary from around 3 m/s to 4.5 m/s; whereas in Table 5, Eq. (13) can accommodate the ship speed as an input ranging from 0.1 m/s to 10 m/s. Moreover, Fig. 26(b) shows that in this particular case, the icebreakers can offer a maximum net thrust (i.e., used to overcome the ice resistance) in the range from around 1.2 MN to 1.8 MN, whereas in Table 5, the range of f_b can be up to 2.07 MN for only one ice breaking event (normally there are several ice breaking events taking place simultaneously around the ship hull for ice – going ships transiting in level ice (Enkvist et al., 1979, Lu et al., 2018)). With this concrete example, we demonstrated that there is a large margin for the use of Eq. (13) when it comes to its engineering applications. Reversely, it should be clarified here that Eq. (13) alone cannot be used to predict ship speed in various ice conditions. Additional information such as the *h-v* curve and net thrust curve as in Fig. 26 are needed for that purpose.

Finally, to check the generality of the ANN model, we performed a sensitivity study of the ice thickness variation. We made a case study between 0.5 m thick and 1.0 m thick ice wedge. A comparison between the ANN model predictions and FEM simulations are presented in Fig. 27. As shown in the sensitivity study, ice thickness influence is well characterized by the ANN model as supposed to be.

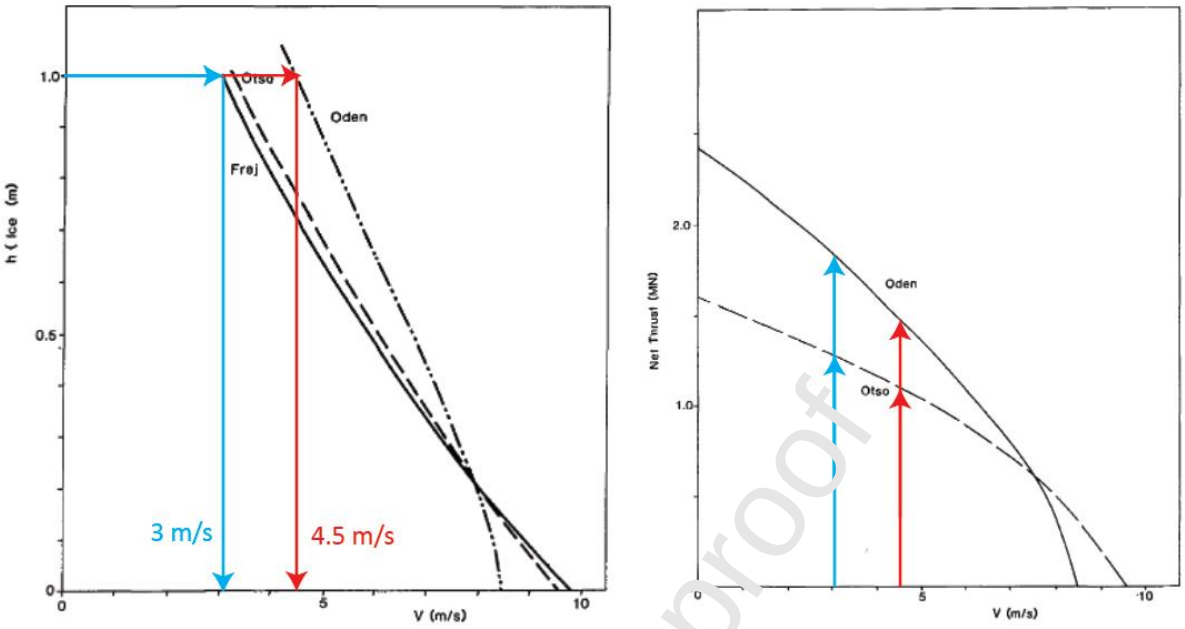

(a) Transit speed vs. ice thickness (b) Transit speed vs. maximum net trust

Fig. 26 Actual engineering case with the icebreaker Otso, Frej and Oden

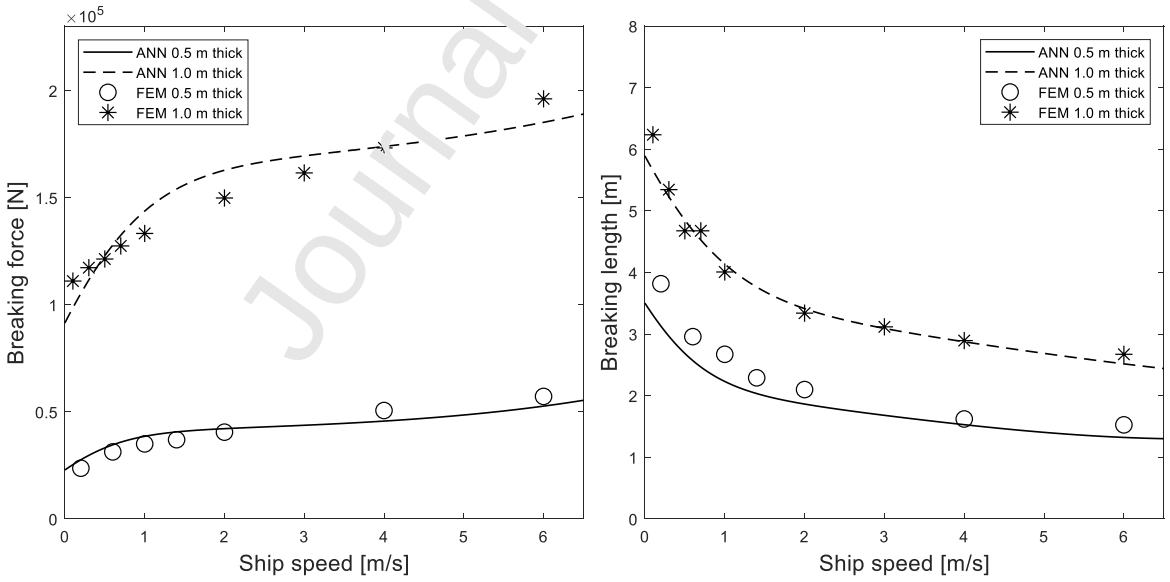

(a) Breaking force (b) Breaking length

Fig. 27 Sensitivity study between 0.5 m thick and 1.0 m thick ice wedge

8. Conclusions

This paper revisits the classic problem of the bending of an ice wedge resting on a Winkler-type elastic foundation. Comparing with previous research efforts, this paper features: 1) studying the dynamic effects; and 2) adopting the Artificial Neural Network (ANN) method to construct a generalized formula that accounts for the dynamic effects, various ice wedge geometries and loading radiuses. These two objectives/features are achieved/realized through two major tasks:

First, a Finite Element Method (FEM) – based model is constructed to numerically solve the ice wedge's bending problem. Before running the dynamic cases, the FEM – based model's static solutions are compared with the analytical static solutions from Nevel (1958, 1972). It is found that:

- There is a generally good agreement between our FEM-based static solution and Nevel's (1972) static solutions in both the ice breaking force and ice breaking length. This signifies our appropriate implementation of the numerical model.
- The best agreement is found for the narrowest ice wedge that was simulated (i.e., with a wedge angle of 30°). This is understandable as Nevel's solution is for 'narrow' wedges (without circumferential deformation).
- The numerical results indicate that the ice breaking force scales with the wedge angle in the form $f_b \propto \theta^{1.15}$. This is different from the often-adopted linear scaling, i.e., $f_b \propto \theta$. On the other hand, the ice breaking length is not too much dependent on the wedge angle (both for the static and dynamic loading scenarios).
- The well-known trend that a larger loading radius or a wider wedge angel leads to both a larger ice breaking force and a longer ice breaking length is re-confirmed quantitatively in Eqs. (7) and (8).
- Moreover, based on the extensive simulation, we identified a wedge angle (i.e., 100°), below which, circumferential crack shall develop first irrespective of the typically encountered loading radiuses. When the wedge angle is larger than this value, a radial crack can take place earlier than the circumferential crack.

Given the satisfactory static analyses and validations, we proceed with the same numerical model and simulated the dynamic scenarios. We varied the ice wedge angles, loading radiuses and the loading rates/interaction

velocity. A total of 1320 simulations are performed, generating a database of 'ice breaking load' and 'ice breaking length', both of which are of great importance in ice – structure interactions. All the simulated results follow/re-confirm the well-known trends. i.e.,

- a faster loading rates leads to a larger ice breaking load and a shorter ice breaking length.
- Moreover, the general trends for the static loading scenarios are magnified in the dynamic case according to the loading rate/interaction velocity. These trends are quantitatively expressed in Eq. (13), which are achieved in the second task.

Second, in order to generalize all the 1320 numerical simulation results, we resort to the ANN method, which is suitable to multivariate and nonlinear problems. Following the ANN recipe, based on the partial FEM – results from the first task, we developed our ANN model in Eq. (13), which is the major contribution from this paper. The equation is expressed in matrix and closed form. We compared our ANN model with: 1) FEM results; 2) existing numerical results from Sawamura et al. (2009, 2014); and 3) experimental data from three icebreakers 'State Island', 'Finncarrier' and 'Jelppari'.

The comparison of Eq. (13)'s prediction with the FEM results indicates that our developed ANN model is of satisfactory engineering accuracy. In response to the accuracy level and physics behind the dynamic bending of an ice wedge, we made a detailed guidance regarding the application range and procedures in using Eq. (13).

The comparisons with the numerical results of Sawamura et al. (2009, 2014) and experimental results of the icebreakers 'State Island', 'Finncarrier' and 'Jelppari' are not exact; mainly due to different numerical setting and field experimental scatters. However, the general trends (presented in Figs. 21-23) of different parameters' influences are well captured by our developed ANN model (Eq. (13)). Based on all these comparisons and a thorough discussion, it is fair to conclude that the developed ANN model allows for easy, efficient and wide engineering applications.

9. Acknowledgement

This research was supported by the MOTIE (Ministry of Trade, Industry, and Energy) in Korea, under the Fostering Global Talents for Innovative Growth Program (P0008747) supervised by the Korea Institute for Advancement of Technology (KIAT). The work is also supported by the Research Council of Norway through the Centres of Excellence funding scheme, project number 203471- NTNU SAMCoT. In addition, the 2nd author would also like to thank VISTA – a basic research programme in collaboration between The Norwegian Academy of Science and Letters, and Equinor, for financial support in writing this paper.

References

ASHTON, G. D. 1986. *River and lake ice engineering*, Water Resources Publication.

BAŽANT, Z. P. Large-scale fracture of sea ice plates. Proc., 11th IAHR Ice Symposium, Banff, Alberta, 1992. Dept. of Civil Engineering, Univ. of Alberta, Edmonton, 991-1005.

BAŽANT, Z. P. & LI, Y. N. 1993. Fracture Analysis of Penetration Through Floating Sea Ice Plate and Size Effect. *ASME APPLIED MECHANICS DIVISION-PUBLICATIONS-AMD,* 163**,** 131-131.

BAŽANT, Z. P. & LI, Y. N. 1994. Penetration fracture of sea ice plate: Simplified analysis and size effect. *Journal of engineering mechanics,* 120**,** 1304-1321.

DEMPSEY, J. P. & ZHAO, Z. G. 1993. Elastohydrodynamic response of an ice sheet to forced sub-surface uplift. *Journal of the Mechanics and Physics of Solids,* 41**,** 487-506.

DEMPSEY, J. P., SLEPYAN, L. I. & SHEKHTMAN, I. I. 1995. Radial cracking with closure. *International journal of fracture,* 73**,** 233-261.

DEMPSEY, J. P., SHEKHTMAN, I. I. & SLEPYAN, L. I. 1998. Closure of a through crack in a plate under bending. *International Journal of Solids and Structures,* 35**,** 4077-4089.

DUDAL, A., SEPTSEAULT, C., BEAL, P.-A., LE YAOUANQ, S. & ROBERTS, B. 2015. A New Arctic Platform Design Tool For Simulating Ice - Structure Interaction. *The 23rd International Conference on Port and Ocean Engineering under Arctic Conditions.* Trondheim, Norway.

ENKVIST, E., VARSTA, P. & RISKA, K. The ship-ice interaction. Proceedings of the 5th International Conference on Port and Ocean Engineering under Arctic Conditions., 1979 Norwegian Institute og Technology, Trondheim, Norway. 977-1002.

Gold, L. W. (1971). Use of ice covers for transportation. Canadian Geotechnical Journal, 8(2), 170-181.

HEATON, J. 2008. Introduction to neural networks with Java. Heaton Research, Inc..

KÄMÄRÄINEN, J. 2007. *Theoretical Investigation on the Effect of Fluid Flow Between the Hull of a Ship and Ice Floes on Ice Resistance in Level Ice*, Helsinki University of Technology, Department of Mechanical Engineering, Laboratory for Mechanics of Materials, Helsinki, Finland.

KEIJDENER, C., HENDRIKSE, H. & METRIKINE, A. 2018. The effect of hydrodynamics on the bending failure of level ice. *Cold Regions Science and Technology,* 153**,** 106-119.

KERR, A. D. 1976. The bearing capacity of floating ice plates subjected to static or quasi-static loads. *Journal of Glaciology,* 17**,** 229-268.

KERR, A. D. & PALMER, L. C. W. 1972. The deformations and stresses in floating ice plates. *Acta Mechanica,*

15**,** 57-72.

KIM, J, KiM, Y., LU, W., 2020. Prediction of ice resistance for ice-going ships in level ice using artificial neural network technique. Ocean Engineering, Volume 217, 108031

KOTRAS, T. V., BAIRD, A. V. & NAEGLE, J. N. Predicting Ship Performance in Level Ice. 1983 New York, NY, USA. SNAME, 329-349.

KOTZ, S., JOHNSON, H. L., & READ, C. B. 1982. Encyclopedia of statistical sciences (No. 519.5 E5)., Encyclopedia of Statistical Sciences, Wiley.

LANGHORNE, P. J., STONE, K. J. L. & SMITH, C. C. 1999. The bearing capacity of saline ice sheets: centrifugal modelling. *Canadian Geotechnical Journal,* 36**,** 467-481.

LI, F., KORGESAAR, M., KUJALA, P., GOERLANDT, F. 2020. Finite element based meta-modeling of ship-ice interaction at shoulder and midship areas for ship performance simulation. Marine Structures, Volume 71, 102736

LI, Y. N. & BAŽANT, Z. P. 1994. Penetration fracture of ice plate: 2D analysis and size effect. *Journal of engineering mechanics,* 120**,** 1481-1498.

LILJA, V.-P., POLOJÄRVI, A., TUHKURI, J. & PAVILAINEN, J. 2019. A free, square, point-loaded ice sheet: A finite element-discrete element approach. *Marine Structures,* 68**,** 102644.

LINDQVIST, G. A straightforward method for calculation of ice resistance of ships. Proceedings of POAC 1989, 1989. 722-735.

LU, W., LØSET, S. & LUBBAD, R. Ventilation and backfill effect during ice-structure interactions. *In:* LI & LU, eds. The 21st IAHR International Symposium on Ice, June 11-15, 2012 2012a Dalian, China. 826-841.

LU, W., LUBBAD, R. & LØSET, S. 2015. Out-of-plane failure of an ice floe: Radial-crack-initiation-controlled fracture. *CRST,* 119**,** 183-203.

LU, W., LUBBAD, R., HØYLAND, K. V. & LØSET, S. 2014. Physical model and theoretical model study of level ice and wide sloping structure interactions. *Cold Regions Science and Technology,* 1**,** 1-33.

LU, W., LUBBAD, R., SHESTOV, A. & LØSET, S. 2018. Parallel channels' fracturing mechanism during ice management operations. Part I: Theory. *CRST***,** 102-116.

LU, W., LUBBAD, R., LØSET, S. & HØYLAND, K. V. Cohesive zone method based simulations of ice wedge bending: a comparative study of element erosion, CEM, DEM and XFEM. *In:* LI & LU, eds. The 21st IAHR International Symposium on Ice, June 11-15, 2012 2012b Dalian, China. 920-938.

LU, W., LUBBAD, R., LØSET, S. & KASHAFUTDINOV, M. 2016. Fracture of an ice floe: Local out-of-plane flexural failures v.s. global in-plane splitting failure. *CRST,* 123**,** 1-13.

LUBBAD, R. & LØSET, S. 2011. A numerical model for real-time simulation of ship-ice interaction. *Cold Regions Science and Technology,* 65**,** 111-127.

MASTERS, T. Practical neural network recipes in C++. Morgan Kaufmann, 1993.

METRIKIN, I. & LØSET, S. Non-Smooth 3D Discrete Element Simulation of a Drillship in Discontinuous Ice. Proceedings of the 22nd International Conference on Port and Ocean Engineering under Arctic Conditions, 2013 Espoo, Finland.

MICHEL, B. 1978. *Ice mechanics,* Quebec, LES PRESSES DE L'UNIVERSITE LAVAL.

NAEGLE, J. N. 1980. *Ice-Resistance Prediction and Motion Simulation For Ships Operating in The Continuous Mode of Icebreaking.* The University of Michigan.

NAIDU, K., ALI, M. S., ABU BAKAR, A. H., TAN, C. K., ARIF, H., & MOKHLIS, H. 2020. Optimized artificial neural network to improve the accuracy of estimated fault impedances and distances for underground distribution system. Plos one, 15(1), e0227494.

NEVEL, D. E. 1958. The theory of a narrow infinite wedge on an elastic foundation. U. S. Army Snow Ice and Permafrost Research Establishment, Corps of Engineering.

JOHANSSON, B. & LILJESTROM, G. 1989. ODEN-A STATE-OF-THE-ART ICEBREAKER. *POAC 89.*

NEVEL, D. E. 1961. The narrow free infinite wedge on an elastic foundation. U. S. Army Snow Ice and Permafrost Research Establishment, Corps of Engineering.

NEVEL, D. E. The ultimate failure of a floating ice sheet. International Association for Hydraulic Research, Ice Symposium, 1972. 17-22.

SAWAMURA, J. Numerical Study on Ice Force Distribution for Plate Ice Failure and Broken Ice Submerging for Ship Maneuver in Level Ice. 22nd IAHR International Symposium on Ice, August 11 to 15, 2014 2014 Singapore. 171-178.

SAWAMURA, J., RISKA, K. & MOAN, T. Finite Element Analysis of Fluid-Ice Interaction during Ice Bending. 19th IAHR International Symposium on Ice, July 6 to 11, 2008 2008 Vancouver, British Columbia, Canada. 239-250.

SAWAMURA, J., RISKA, K. & MOAN, T. 2009. Numerical Simulation of Breaking Patterns in Level Ice at Ship's Bow. *Proceedings of the Nineteenth (2009) International Offshore and Polar Engineering Conference.* Osaka, Japan.

SAWAMURA, J., TACHIBANA, T., TSUCHIYA, H. & OSAWA, N. Numericial Investigation for the Bending Failure of Wedge-Shaped Floating Ice. 20th IAHR International Symposium on Ice, June 14 to 18, 2010 2010 Lahti, Finland.

SEPTSEAULT, C., BÉAL, P.-A., LE YAOUANQ, S., DUDAL, A. & ROBERTS, B. 2014. A New Ice Simulation Tool Using a Multi-Model Program. Offshore Technology Conference.

Sharifi, A., & Mohebbi, A. 2012. Introducing a new formula based on an artificial neural network for prediction of droplet size in venturi scrubbers. Brazilian Journal of Chemical Engineering, 29, 549-558.

SODHI, D. S. 1995. Breakthrough loads of floating ice sheets. *Journal of cold regions engineering,* 9**,** 4.

SODHI, D. S. 1997. Vertical penetration of floating ice sheets. *International Journal of Solids and Structures,* 35**,** 4275-4294.

SODHI, D. S., KATO, K., HAYNES, F. D. & HIRAYAMA, K. 1982. Determining the characteristic length of model ice sheets. *Cold Regions Science and Technology,* 6**,** 99-104.

SQUIRE, V. A., HOSKING, R. J., KERR, A. D. & LANGHORNE, P. J. 1996. *Moving loads on ice plates*, Springer.

STATHAKIS, D. 2009. How many hidden layers and nodes?. International Journal of Remote Sensing, 30(8), 2133-2147.

SU, B., RISKA, K. & MOAN, T. 2010a. A numerical method for the prediction of ship performance in level ice. *Cold Regions Science and Technology,* 60**,** 177-188.

SU, B., RISKA, K. & MOAN, T. 2010b. Numerical simulation of local ice loads in uniform and randomly varying ice conditions. *Cold Regions Science and Technology*.

SU, B., RISKA, K. & MOAN, T. Numerical simulation of ship turning in level ice. PROCEEDINGS OF THE ASME 29TH INTERNATIONAL CONFERENCE ON OCEAN, OFFSHORE AND ARCTIC ENGINEERING, 2010, VOL 4, 2010c. AMER SOC MECHANICAL ENGINEERS, 751-758.

TAN, X., SU, B., RISKA, K. & MOAN, T. 2013. A six-degrees-of-freedom numerical model for level ice–ship interaction. *Cold Regions Science and Technology,* 92**,** 1-16.

VALANTO, P. 2001. The resistance of ships in level ice. *SNAME,* 109**,** 53-83.

ZHOU, L., SU, B., RISKA, K. & MOAN, T. 2011. Numerical simulation of moored structure station keeping in level ice. *Cold Regions Science and Technology*.

Author statements

Jeong-Hwan Kim: Data curation, Investigation, Formal analysis, Visualization, Writing- Original draft preparation; **Wenjun Lu**: Conceptualization, Investigation, Methodology, Writing- Original draft preparation, Writing- Reviewing and Editing; **Raed Lubbad**: Conceptualization, Supervision; **Sveinung Løset**: Supervision, Funding acquisition; **Beom-Seon Jang**: Supervision, Funding acquisition.

Declaration of interests

☒ The authors declare that they have no known competing financial interests or personal relationships that could have appeared to influence the work reported in this paper.

☐The authors declare the following financial interests/personal relationships which may be considered as potential competing interests:

Highlights

- Extensive finite element method – based simulations on the dynamic bending of an ice wedge resting on a Winkler-type elastic foundation are conducted based on inputs (i.e., ice wedge geometry, loading radius and loading rate) within ranges that are typical for engineering applications.
- Based on the simulation, a database of 'ice breaking load' and 'ice breaking length' is constructed. Then we applied the artificial neural network method to establish the general relationship between the varying inputs with the target outputs.
- Such relationship is expressed in simple closed-form allowing for easy, efficient and wide engineering applications.